WILEY-VCH

DOI: 10.1002/ ((please add manuscript number))

Progress Report

Synthetic Two-Dimensional Materials: A New Paradigm of Membranes for Ultimate Separation

*Zhikun Zheng, Ronny Grünker, Xinliang Feng**

Dr. Z. Zheng 1, Dr. R. Grünker 1, Prof. X. Feng 1
Department of Chemistry and Food Chemistry, Center for Advancing Electronics Dresden (CFAED), Technische Universität Dresden, 01069 Dresden, Germany
E-mail: xinliang.feng@tu-dresden.de

Keywords: Functional materials, gas separation, membrane, two-dimensional materials, water desalination

Abstract: Microporous membranes act as selective barriers and play an important role in industrial gas separation and water purification. The permeability of such membranes is inversely proportional to their thickness. Synthetic two-dimensional materials (2DMs), with a thickness of one to a few atoms or monomer-units are ideal candidates for developing separation membranes. In this Progress Report, we present groundbreaking advances in the design, synthesis, processing, and application of 2DMs for gas and ion separations, as well as water desalination. After the introduction in Section 1, this report describes the syntheses, structures, and mechanical properties of 2DMs in Section 2. In Section 3, we will discuss the established methods for processing 2DMs into selective permeation membranes and address the separation mechanism and their performances. Finally, current challenges and emerging research directions, which need to be addressed for developing next generation separation membranes, are summarized in the Conclusion and Perspective.

1. Introduction

Separation is widely used in industry to recover pure gas, capture greenhouse gas, and supply fresh water. Compared with conventional separation methods, such as cryogenic and adsorptive or absorptive gas separation, as well as thermal desalination, membrane separation

is an energy-efficient and environment-friendly technique, which occupies less space and can be operated in a continuous mode.[1] An ideal membrane should be as thin as possible to maximize flux, as selective as possible to enable efficient separation, and as mechanically robust as possible to prevent membrane rupture.

Microporous membranes fabricated from linear polymers show a variety of structural and dynamic behavior, leading to a range of permeation properties. However, the performances of such membranes are subject to a trade-off between selectivity and permeability, known as Robeson's upper bound.[2] Inorganic membranes using zeolites or metal organic frameworks (MOFs) show good performances due to their porous structures and sieving capabilities based on the pores. Unfortunately, zeolite and MOF membranes have failed to be produced economically on a large scale due to high engineering cost, uncontrolled defect formation, and poor reproducibility during membrane production.[3] In the past two decades, there has been considerable interest in carbon nanotubes (CNTs) because of their unique one-dimensional nanochannels and extremely strong mechanical properties.[4] However, it is technically challenging and energy-demanding to achieve high-density, vertically aligned CNT membranes on a large scale. Overall, current microporous membranes are generally thicker than 20 nm to minimize undesirable flux contribution through non-selective defects to maintain a reasonably high separation selectivity.

In the past decade, the advent of graphene, i.e., a 2D atomic layer of sp^2 carbons, has inspired the synthesis of various 2D materials (2DMs), including graphene oxide (GO), 2D polymers and supramolecular polymers (2DPs and 2DSPs; they are laterally infinite, one-monomer unit thick, freestanding networks with defined internal periodicity based on covalent or non-covalent bonds, respectively), 2D MOFs, and carbon nanomembranes (CNMs).[5] These materials have opened a new era of membranes due to their hyper-thinness, which minimizes transport resistance and maximize flux, offering ultimate separation capabilities. Moreover, 2DMs can exhibit precisely defined porous structures and/or chemical functionalities, which

enable their extraordinary separation selectivities. Furthermore, 2D materials can be readily assembled into layered stacks with a well-defined interlayer distance, which act as separation channels. Finally, excellent mechanical, chemical, and thermal stabilities of 2DMs guarantee their practical applications.

In this Progress Report, we present recent breakthrough advancements in the synthesis and fabrication of synthetic 2DMs favorable for gas and ion separations, as well as water desalination. Particular emphasis will be given to synthetic 2DMs, such as functional graphene oxide, 2DPs and 2DSPs, 2D MOFs, and carbon nanomembranes with the focus on the development of novel materials and methods for processing them into separation membranes. Other inorganic sheets, such as metal chalcogenides and boron nitride, have been widely explored for electronics but have seldom been used for separation purposes; hence, they will not be covered in this report.

2. Synthesis, structure and mechanical properties of 2DMs

2.1. Graphene

Graphene is a planar 2D material with a hexagonal carbon lattice. It has a geometric pore size of 0.64 Å (Figure 1) and is one order of magnitude smaller than the van der Waals radius of a He atom (2.6 Å), which is the smallest gas. Graphene has a high mechanical strength (130 GPa) and Young's modulus (1 TPa), which are comparable or even superior to those of carbon nanotubes.[6]

Pristine graphene is an excellent starting material for developing size-selective separation membranes because of its atomic thickness, high mechanical robustness, and impermeability to all gases. Graphene produced by mechanical cleavage and chemical vapor deposition (CVD) has been explored for gas permeation and water purification/desalination.[7] Both methods can produce single crystalline graphene (defect-free) with sizes of 100 μm^2 (mechanical cleavage)[5a] up to 1 cm^2 on copper foils and on silicon wafers with hydrogen-

terminated germanium buffer layers (CVD).[8] Moreover, the CVD process can create polycrystalline graphene with very large areas (side length ≈75 cm) on copper foil.[9] The prepared graphene samples can be readily transferred onto holey substrates via poly(methyl methacrylate) or thermal tape mediated transfer,[10] enabling their integrations into membrane technologies.

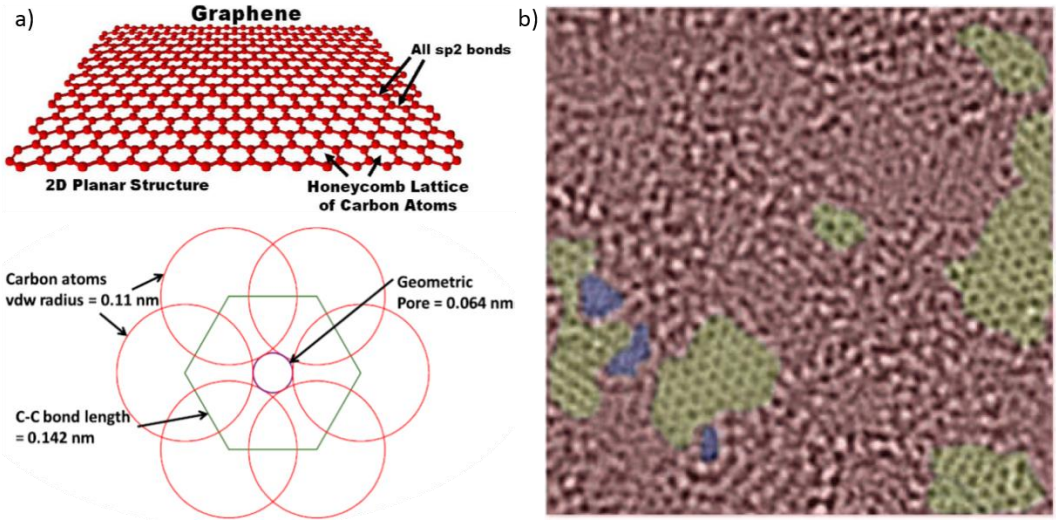

Figure 1. a) Graphene lattice structure. Reproduced with permission.[11] Copyright 2013, Elsevier. b) TEM image of suspended GO sheet; holes, graphite areas, and oxidized regions are marked in blue, yellow, and red, respectively. Reproduced with permission.[12] Copyright 2010, Wiley-VCH.

2.2. Synthetic 2DMs

In this section, we will present several representative synthetic 2D materials, such as functional graphene oxide, 2DPs, 2DSPs, 2D MOFs, and carbon nanomembranes. Their synthetic methods, structures, and mechanical properties will be briefly described here.

2.2.1. Graphene Oxide

GO can be regarded as the oxidized form of graphene, having a high density of oxygen-containing functional groups, such as carboxylate, hydroxyl, and epoxy groups. Transmission electron microscopy image of GO shows disordered oxidized regions of the basal plane

forming a continuous network with small isolated aromatic species (graphitic region, up to 8 nm^2) and holes (usually under 5 nm^2) (Figure 1b).[12] As the coverage of the oxidized regions and holes increase, both the Young's modulus and intrinsic strength decrease monotonically due to the disturbance of sp^3 carbons (breaking of the sp^2 carbon network and lowering the energetic stability). Nevertheless, typical GO shows a Young's modulus of ~ 207.6 GPa,[13] similar to that of stainless steel. In comparison with CVD and mechanically exfoliated graphene, GO can be cheaply produced on a large scale by the oxidation of graphite with subsequent exfoliation to obtain individual layers.[5b, 14] The most acknowledged method to synthesize GO is developed by Hummers in 1958, in which graphite is oxidized by 3 mol L^{-1} $KMnO_4$ and 0.5 mol L^{-1} $NaNO_3$ in concentrated H_2SO_4.[15] A modification of Hummers' method with 6 mol L^{-1} $KMnO_4$ as the oxidant has also been widely used. As a result of such harsh oxidation condition, GO is highly hydrophilic and can be dispersed in water as macroscopic flakes. This makes GO compatible with various membrane processing methods and facilitate its applications in membranes.

2.2.2. Two-dimensional Polymers

To be a potential building block for the synthesis of a linear polymer, the monomer needs to have two latent sites capable of bond formation (Figure 2a). In contrast, for the synthesis of 2DPs, shape-persistent monomers are required, having at least three latent sites capable of bond formation to connect to three other (same or different) building blocks (Figure 2b). A 2DP can be regarded as a series of n-strand ladder chains (n depends on the lateral size of the 2DP), where breaking/damaging single or multiple chains will not affect its properties significantly, and it exists as long as not all of its chains along a line are disconnected, leading to improved mechanical, chemical, and thermal stabilities. This makes 2DPs in principle better separation membranes than their 1D analogues (vide infra).

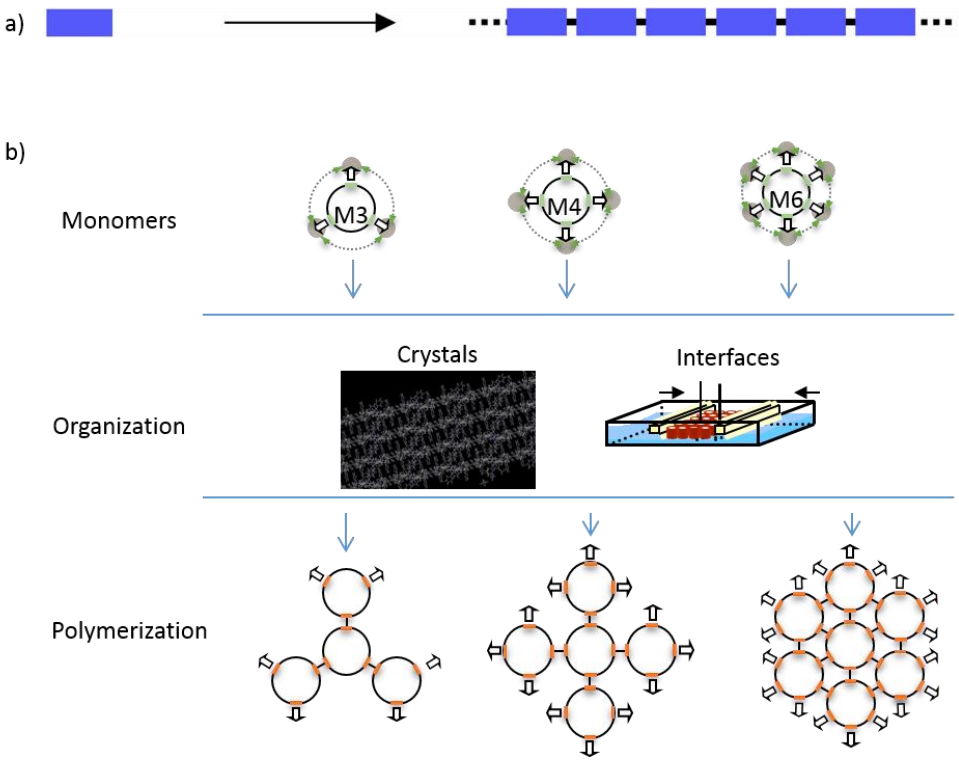

Figure 2. Schematic illustration for the synthesis of a) linear polymers and b) 2DPs/2DSPs with rigid and symmetric monomers at the interfaces. Crystal and air-water interfaces are used as examples to confine monomers in two dimensions.

In general, there are two strategies to prepare 2DPs: top-down exfoliation and bottom-up assembly. The top-down approach typically involves solution or solid exfoliation/delamination of a laminar structure to generate single-layered 2DPs. For example, in 2012, the first synthesis of a 2DP using a three step strategy was reported by Schlüter and co-workers. This strategy includes the arrangement of predesigned monomers in a laminar crystal followed by photochemically induced lateral cross-linking with subsequent exfoliation into monolayer sheets (Figure 3a, 3b).[16] Following this concept using monomer **1**, a nanoporous 2DP with a thickness of ~ 1 nm was obtained in 2014. This type of 2DP has precisely defined monodisperse pores of ~ 0.9 nm and a high pore density of 3.3×10^{13} pores cm^{-2}.[17]

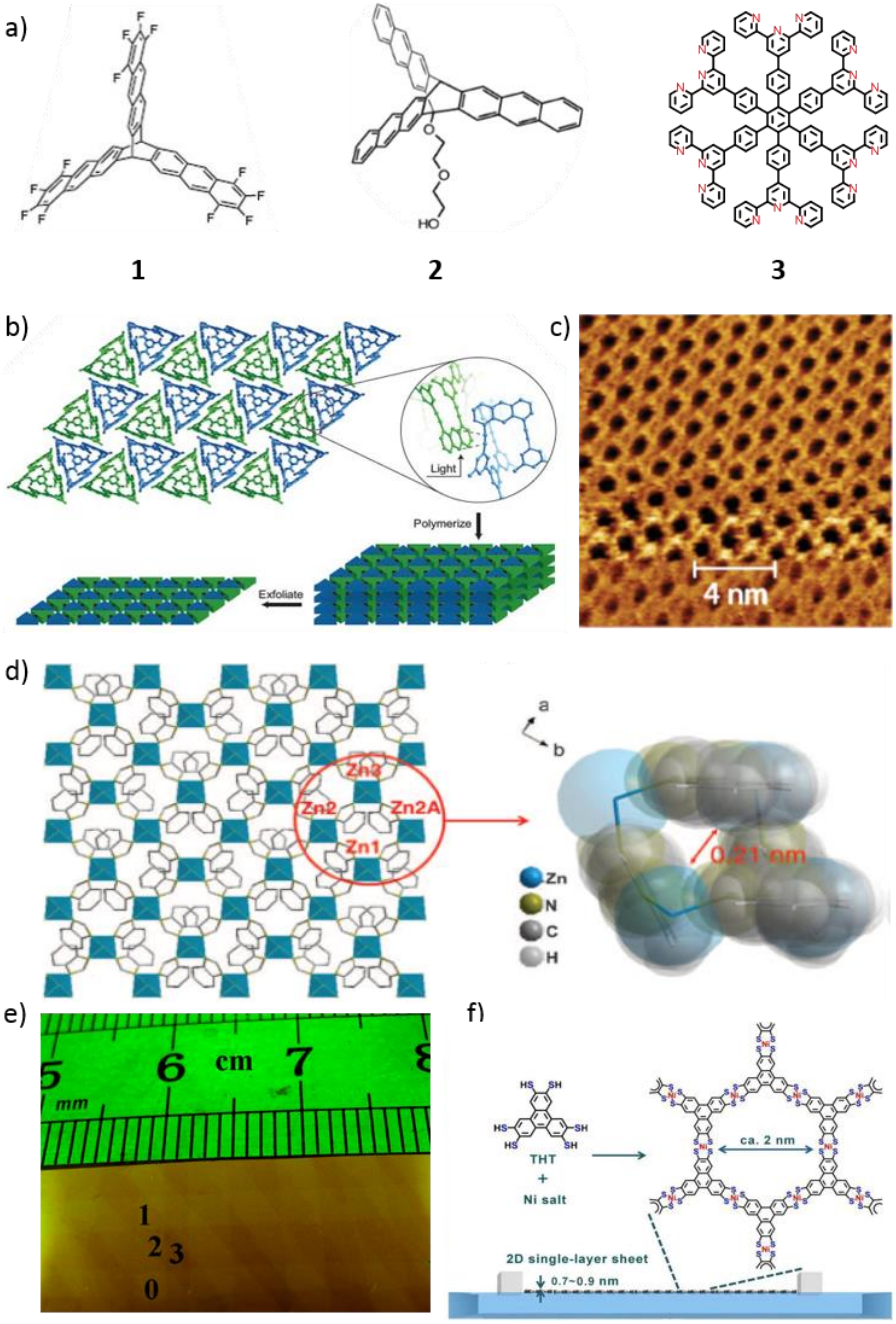

Figure 3. Representative examples of 2DPs, 2DSPs, and 2DMOFs. a) Chemical structure of monomers **1** – **3**.[17-18] b) Schematic illustration to achieve 2DPs with top-down exfoliation from laminar crystals. Reproduced with permission.[16] Copyright 2012, Macmillan Publishers Limited. c) Scanning tunneling microscope image of a 2DP from monomer **2** on highly oriented pyrolytic graphite (HOPG). Reproduced with permission.[18a] Copyright 2014, American Chemical Society. d) Structure and pore size illustrations of a 2D Zn_2(benzimidazole)$_4$. Reproduced with permission.[19] Copyright 2015, the American Association for the Advancement of Science. e) Optical microscopy image of stacked 2DSP stripes from monomer **3**. The number of 2DSP strips is indicated. Reproduced with

permission.[20] Copyright 2013, Wiley-VCH. f) Synthesis of a 2DSP composed of triphenylene-fused nickel bis(dithiolene) complexes through the Langmuir-Blodgett method at an air/water interface. Reproduced with permission.[21] Copyright 2015, Wiley-VCH.

Alternatively, the bottom-up assembly is based on the polymerization of designed monomers confined in two dimensions. Ultra-high vacuum assisted interfacial synthesis has been widely explored for this purpose.[22] However, the synthesized compound is limited to nanometers in size due to the poor diffusion of monomers on a solid surface, and the transfer of such structures from its original substrate for usage as membranes is challenging. To achieve 2DPs with a large lateral size, interfaces that allow unlimited diffusion of monomers, such as the air-water interface of a Langmuir-Blodgett trough, are used to guide the organization of the monomers in two dimensions (Figure 2b).[18a, 23] To this end, amphiphilic monomers are studied and are expected to spread at the air-water interface. The hydrophobic part will be exposed to the air, whereas the hydrophilic part stays in the water subphase. The reactive groups at the periphery of the monomers would reside at approximately the same height above the interface and facilitate their reactions with each other. For instance, polymerization of compound **2** by UV-irradiation at the air-water interface leads to a porous 2DP (6.8×10^{13} pores/cm^2, ~30% open area) with a thickness of ~ 1.2 nm and a pore size of ~ 0.7 nm (Figure 3c). The achieved 2DP has a lateral size of ~ 1 cm^2 on a solid substrate and can be freely suspended over 20 μm × 20 μm sized holes.[18a]

2.2.3. Two-dimensional Supramolecular Polymers and 2D Metal-Organic Frameworks

In the last section, the synthesis of 2DPs based on the formation of covalent bonds has been discussed. Recent studies have shown that through non-covalent bonds, especially coordination and host-guest interactions, 2DSPs with structure and topology similar to that of

2DPs can also be constructed.[18b, 19-21, 24] Moreover, 2DSPs based on the formation of coordination bonds can also be regarded as 2D MOFs.

Similar to the synthesis of 2DPs, 2DSPs/2D MOFs can also be obtained by either top-down exfoliation or bottom-up protocols.[19, 24d-g] The starting materials for the top-down protocol are laminar MOFs, which can be exfoliated into single layers with sonication, excess solvent, and wet ball-milling. For instance, individual layers of $[Cu_2Br(IN)_2]_n$ (IN = isonicotinato) has been obtained in 2010 by sonication-assisted delamination, which has a lateral size in the range of hundreds of nanometers and a thickness of 0.5 nm. However, the freestanding behavior of the exfoliated 2D MOFs is not clear, and sonication that is strong enough to break interlayer interactions resulted in defect generation and structural degradation, which hinders the application of the material as separation membranes. Later, the same group synthesized a new laminar MOF with the formula $[Cu(\mu\text{-}pym_2S_2)(\mu\text{-}Cl)]_n$ ($PymS_2$ = dipyrimidindisulfide), which showed an interlayer interaction so weak that it can be delaminated by just the interaction with excess solvent.[24h, 24i] Single layers of MOF with areas of hundreds of square microns were obtained by simple immersion in water, and they can be freely suspended over holes and demonstrated a Young's modulus of ~ 4 GPa. Alternatively, wet ball-milling of Zn_2(benzimidazole)$_4$ crystals at a very low speed (60 rpm) followed by exfoliation in a mixture of methanol and propanol can lead to freestanding crystalline single layers with a pore size of ~ 2.1 Å (Figure 3d).[19] The efficient pore size is slightly large due to the structural flexibility of the 2D MOF caused by the formation of weak bond strengths (in comparison with dithiolene-metal and terpyridine-metal bonds, vide infra) and a distorted coordination geometry around the Zn-centers in the MOF. Nevertheless, the 2D MOF remains stable up to 200°C, as indicated by thermal analysis.

2DSPs/2D MOFs can also be created by bottom-up assembly protocols. When symmetric monomers such as **3** are spread at the air-water interface, coordination between the terpyridine units at its periphery and metal ions, such as Zn^{2+}, Fe^{2+}, Co^{2+}, and Pb^{2+}, will push forward the

formation of 2DSPs with a thickness ranging from 1.4 to 1.9 nm.[18b, 20, 24a] The 2DSPs have a lateral size of several cm^2 on a solid substrate (Figure 3e) and can be freely suspended over 20 μm × 20 μm sized holes. The Young's modulus of the iron-based 2DSP is ~ 16 GPa. Interestingly, the coordination between terpyridine and Zn^{2+} is reversible, whereas it is irreversible for other metal ions. The reversible coordination reaction provides the possibility to anneal structural defects, thus achieving the highest possible order within the sheets. On the other hand, reversible complexes have less bond strengths, resulting in fragile Zn-based 2DSPs. Interestingly, Zn^{2+} in Zn-based net points can be replaced with other metal ions by post-synthetic transmetalation, resulting in isostructural and more stable sheets.[18b] In addition to the terpyridine-metal coordination, carboxyl-, bis(dipyrinato)-, and dithiolene-metal coordinations have also been explored for the synthesis of 2DSPs/2D MOFs at an air-water interface.[21, 24b-d] Among the available chemical methodologies, dithiolene-metal coordination is especially interesting because it forms planar bonds which are strong enough to freely suspend the synthesized 2DSPs/2D MOFs over holes. Recently, we demonstrated the integration of large π-delocalized polycyclic aromatic hydrocarbons into 2DSP based on the coordinative assembly of 1,2,5,6,9,10-triphenylenehexathiol with nickel salt at an air-water interface (Figure 3f).[21, 25] The resulting 2DSP has a thickness of ~ 0.7 nm and a lateral size in the range of mm^2. Selected-area electron diffraction confirmed that the 2DSP has a long-range order with a lattice constant of approximately 2.0 nm. Importantly, such 2DSPs showed excellent electrocatalytic activities towards hydrogen evolution reactions (HERs), which were superior to those reported for carbon nanotube (CNT)-supported molecular catalysts and heteroatom-doped graphene catalysts.[26] It is assumed that when such porous polymer sheets capable of producing gas are employed, gas can be generated and purified simultaneously.

An elegant example for the formation of 2DSP based on host-guest enhanced interactions was recently demonstrated by us with a monomer consisting of a tris(methoxynaphthyl)-substituted truxene spacer and a naphthalene diimide substituted with N-methyl viologenyl

moieties as donor and acceptor monomers, respectively, in combination with cucurbit[8]uril as a host monomer.[24j] Featuring orthogonal solubility, the participating monomers can self-assemble at a liquid − liquid interface, yielding a 2DSP with a thickness of 1.8 nm, homogeneously covering areas up to 0.25 cm^2, and featuring the ability to be freestanding over holes of 10 μm^2.

2.2.4. Carbon Nanomembranes

CNMs are generally obtained by covalently cross-linking densely compacted monolayers of molecules, such as self-assembled monolayers (SAMs), on the surface. In the very best situation, self-assembled molecules attain a 2D crystalline order and are packed at van der Waals distances. Irrespective of the cross-coupling mechanism, this distance of approximately 3.5 Å will be reduced to the length of a covalent bond, which is on the order of 1.5 Å.[5c] The molecules can deform or collapse to compensate for the bond shrinkage, resulting in pore formation. Because SAMs can grow as large as allowed by the sample size, large-area (cm^2) CNMs can be produced. For instance, electron irradiation of SAMs of 4′-nitro-1,1′-biphenyl-4-thiol (NBPT) and 4′-carbonnitrile-1,1′-biphenyl-4-propyltrimethoxysilane leads to unimolecular nanomembranes, which can be released from their substrates and transferred onto holey substrates. Such membranes have a thickness of ~ 1 nm and lateral size of up to several cm^2.[5d, 27] The NBPT membrane has two distinct faces possessing amino- and thiol-groups, which can be chemically functionalized independently.[28] It is worth noting that chemical functionalization does not lead to a change in the integral structure of the membrane; thus, the initial mechanical properties are retained.[29] Moreover, the thickness and Young's moduli of such CNMs can vary from ~ 0.5 nm to ~3 nm and ~ 9 – 19 GPa, respectively, depending on the selection of the precursor monomers for the formation of SAMs (Figure 4).[27a] When bulky molecules (Figures 3h and 3i) are used for the preparation of SAMs, steric hindrance causes a less packing density. Thus, once such SAMs are cross-

linked, randomly distributed pores with sizes of ~ 1 - 10 nm are obtained as indicated by helium ion microscopic images. Similarly, ultraviolet-induced cross-linking of SAMs of a hexayne-containing amphiphilic monomer at the air-water interface of a Langmuir-Blodgett trough leads to the formation of a CNM with a thickness of 1 - 2 nm.[30]

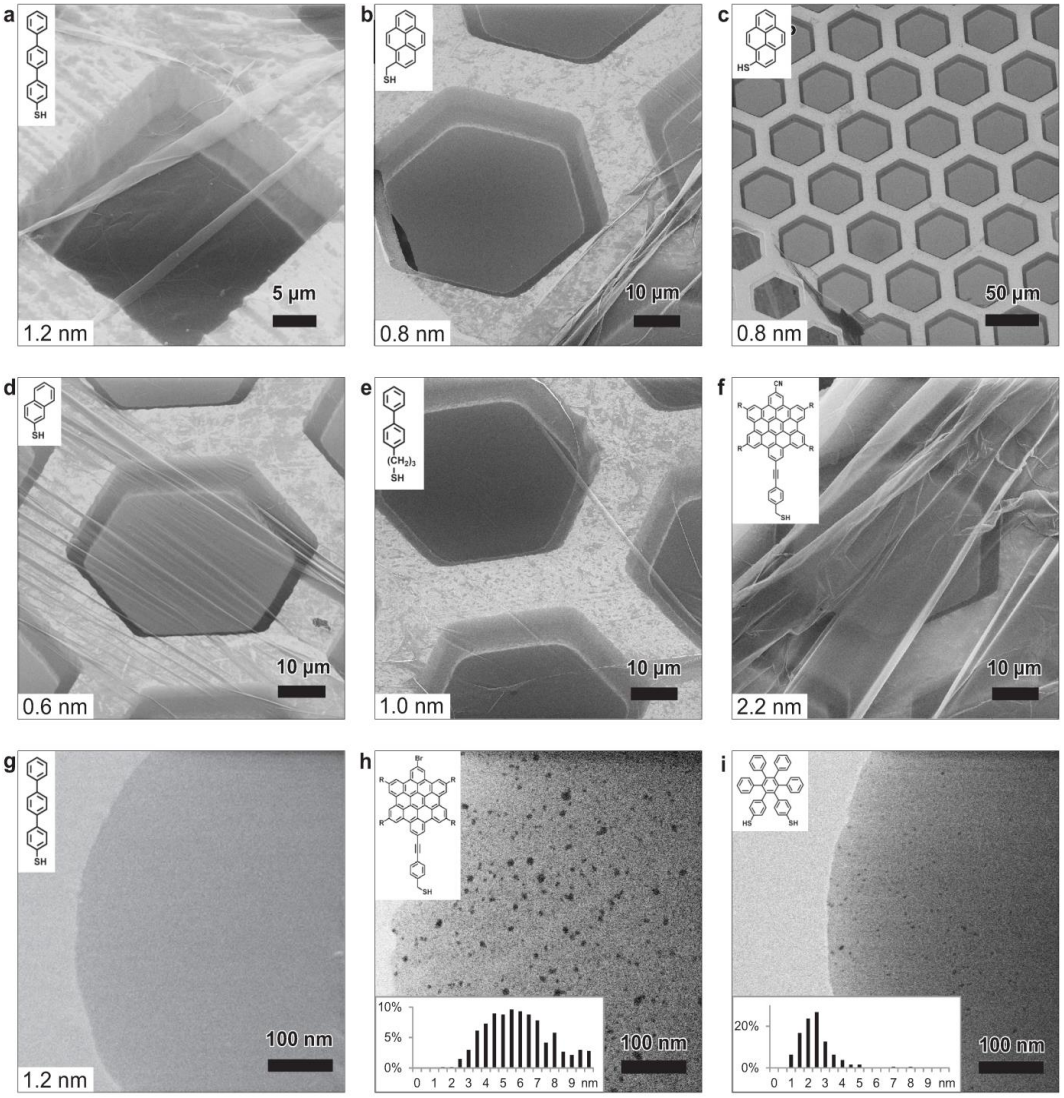

Figure 4. Helium ion microscope (HIM) micrographs of free-standing CNMs. The upper left insets show the precursor molecules. The CNM in (a) is suspended over a gold TEM grid. CNMs in (b-f) are over copper grids and CNMs in (g-i) are over Cu grids with thin carbon films. The numbers in the lower left corners indicate the CNM thicknesses. HIM images (h and i) show CNMs with nanopores; the lower insets show the respective distributions (in %) of the pore diameters (in nm). Reproduced with permission.[27a] Copyright 2013, American Chemical Society.

3. Application in Gas Separation

3.1. Synthetic 2DMs

For use as separation membranes, 2DMs can be processed into two forms: porous membranes and layered stacks. Methods on the generation of pores with different sizes and density, the process of 2DMs into laminates, and the control of the interlayer structure of the laminates are summarized in the following section.

3.1.1. Porous Membranes

Due to enthalpy effects, nature avoids vacuum, which means that the formation of pores is energetically unfavorable. For the controlled creation of intrinsic pores within a material, one has to avoid the formation of dense phases, e.g., by using rigid monomers bearing intrinsic open spaces, which are true for the syntheses of 2DPs, 2DSPs, and 2D MOFs. The sizes of pores within these materials could be rationally tuned by varying the size and geometry of the monomers, which would allow the synthesis of porous membranes for specific separations. On the other hand, if the size of the pores within a material is too small to be used for gas separation (such as in the case of graphene), size-selective pores need to be introduced. To this end, various techniques have been developed, such as electron beam irradiation,[31] oxidative etching,[7a] ion-beam bombarding,[7b] plasma,[7e, 32] block copolymer and nanosphere lithography,[33] catalytic hydrogenation,[34] and combinations of these techniques.[35] In this section, techniques that lead to the generation of pores with diameters ≤ 10 nm, as well as pores with diameters > 10 nm, for the exploration of gas permeation will be discussed.

Nanometer-sized pores can be generated in graphene with electron beam irradiation at room temperature. The electron beam used for this purpose normally has a very high energy (hundreds of KeV).[31] The exact value of the minimum energy required to remove an atom from the interior of a sp^2-carbon lattice to create pores is still controversial. Generally, 80 KeV is below the threshold. However, graphene nanopores with radii as small as 0.3 nm can

be generated by inducing defect nucleation centers with energetic ions (such as 3 KeV Argon ions) and subsequently eliminating carbon atoms at the edge of the centers with a uniform defocused electron beam of 80 KeV.[35b] Graphene nanopores (< 10 nm) can also be produced using low-energy (< 10 KeV) focused electron beam in a scanning electron microscope (SEM) in the presence of nitrogen gas. In this case, nitrogen gas is ionized by the beam, enabling its bonding with carbon atoms to form a gaseous product (cyanogen), which is pumped from the system and leads to the formation of pores.[36] In the above-mentioned cases, however, only the generation of a few pores is demonstrated. Recently, millions of pores were drilled in bilayer graphene using focused ion beam. Low exposure doses of Ga^+ (5×10^{-6} to 5×10^{-5} pA/nm^2) and He^+ (6×10^{-3} pA/nm^2) ions enable fast and precise production of well-defined pores with narrowly distributed diameters in the range of < 10 nm and 14 nm – 1 μm, respectively (Figure 5a).[7b] Nevertheless, the sizes of the pores are far from subnanometers, which are crucial for sieving gases and ions.

Alternatively, randomly distributed pores can be generated in large areas with other techniques. Subnanometer-sized pores in graphene can be introduced by first creating reactive defects sites with ion bombardment and subsequent enlargement by chemical oxidation etching. The size of the pores is 0.4 nm ±0.24 nm with density exceeding 10^{12} cm^{-2} (Figure 5b).[35a] Ultraviolet-induced oxidative etching can also introduce subnanometer-sized pores (~ 0.34 nm and ~ 0.49 nm) directly in graphene, and the resulting membranes can be used as molecular sieves.[7a] Moreover, subnanometer-sized pores in monocrystalline graphene sheets can be produced by O_2 plasma irradiation. The size and density of the pores can be increased by increasing the plasma etching time. At an etching time of ~ 1.5 s, pores with a diameter of ~ 0.5 – 1 nm and a density of ~ 10^{10} cm^{-2} are obtained.[7e]

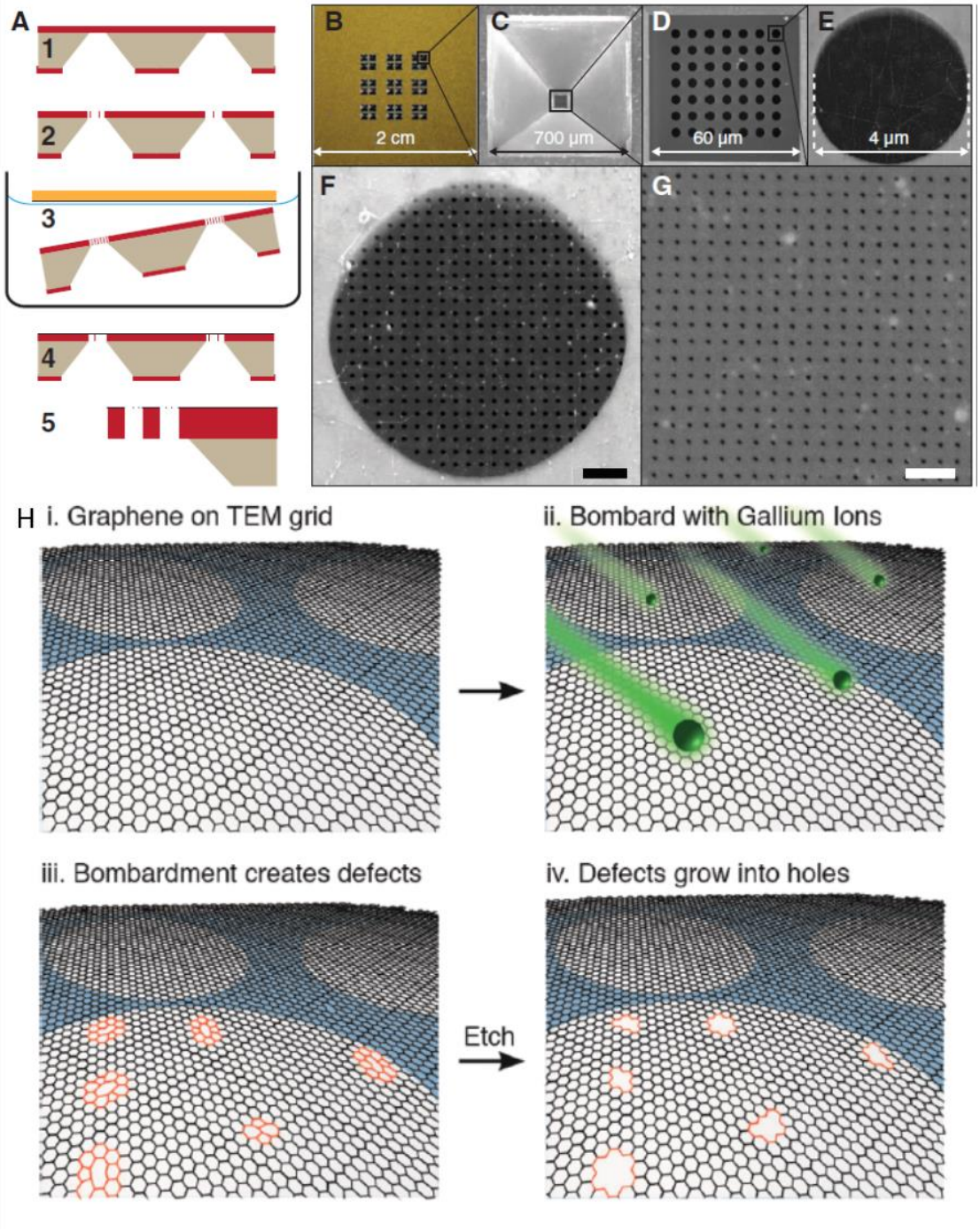

Figure 5. Process to create ordered (A-G) and randomly-distributed (H) pores in graphene membranes. (A) Schematic of the porous graphene fabrication process. Step 1: Freestanding SiNx membrane formation. Step 2: Microscale pore formation through the SiNx membrane. Step 3: Graphene transfer. Step 4: Graphene surface cleanup. Step 5: physical perforation of graphene (by means of Ga- and He-based FIB drilling). (B) Photograph (bottom view) of a full-membrane structure. (C) Bottom view SEM image of the SiNx membrane. (D to G) Top view SEM images of (D) porous freestanding SiNx window before graphene transfer, (E) freestanding graphene on SiNx open pores, (F) 50-nm-wide

apertures on the freestanding graphene (scale bar, 500 nm), and (G) 7.6-nm-wide apertures (scale bar = 100 nm). Reproduced with permission.[7b] Copyright 2014, American Association for the Advancement of Science. H) Subnanometer pores in graphene are created by ion bombardment followed by chemical oxidation. Reproduced with permission.[35a] Copyright 2014, American Chemical Society.

3.1.2. Layered Stacks

Alternative to the use of predesigned porous sheets, 2DMs can be readily assembled into layered stacks with a well-defined interlayer distance, which can act as separation channels. In this section, we will discuss the various processing methods for the fabrication of stacked layers useful for gas and ion separations, as well as water desalination (Figure 6).

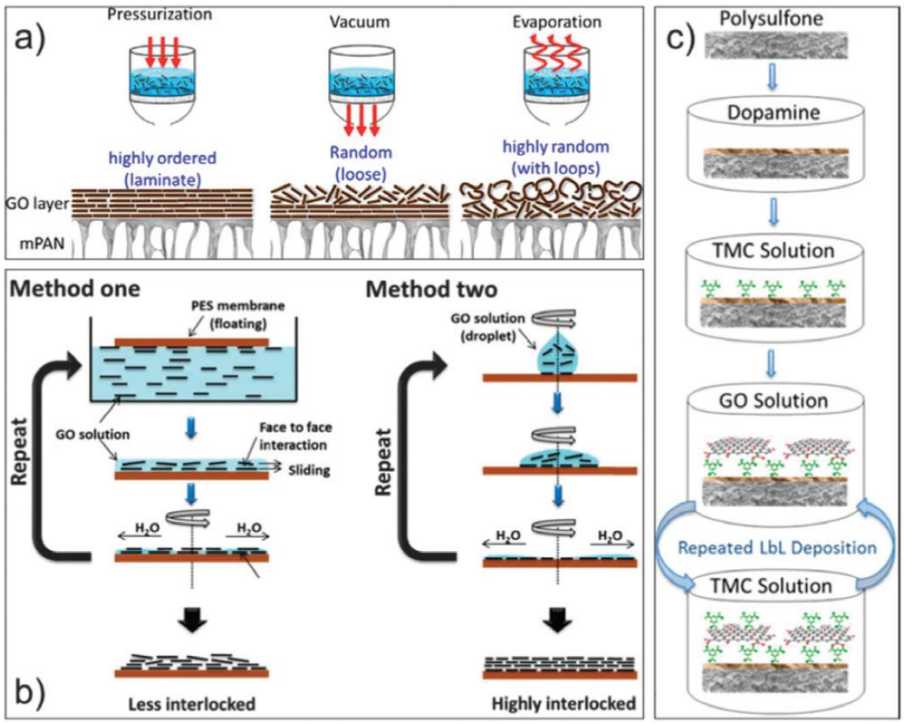

Figure 6. Processing methods for the fabrication of stacked layers by different methods: (a) pressure-assisted self-assembly, vacuum-assisted self-assembly, and evaporation-assisted self-assembly, (b) spin-coating methods, and (c) layer-by-layer method. Reproduced with permission.[37] Copyright 2015, Royal Society of Chemistry.

Processing Methods

Filtration method. Water suspensions of GO sheets can be filtrated to form an interlocked layered structure.[7c, 38] The water flow in the confined space, together with electrostatic, hydrogen bond, and van der Waals interactions between the strong and flexible GO with large aspect ratios, is mainly responsible for the sequential deposition into laminar structures. The thickness of the laminates can be varied using GO sheets with different concentrations and ranges from 1.8 nm to tens of micrometers.[7c, 38a, 38b] The orientation of the GO in the laminates can be tuned by applying different driving forces for the filtration. Pressure-, vacuum-, and evaporation-assisted techniques lead to highly ordered, random, and highly random formations with some loop patterns, respectively (Figure 6a).[38d] X-ray diffraction indicates that the interlayer spacing of the laminates ranges from ~ 8 Å to ~ 14 Å (including the van der Waals thickness of graphene; thickness for reduced GO is ~4 Å; electronic clouds around graphene sheets extend over a distance of ~ 3.5 Å).[38a, 38d, 39]

Coating method. Various coating methods have been reported to assemble GO into laminar membranes, including spin-coating, spray-coating, and drop-casting.[7c, 40] GO membranes with thicknesses varying from 0.1 to 10 μm can be produced by the spin- or spray-coating method.[40a] Thus, the prepared membrane has a layer-to-layer distance of ~10 Å. Drop-casting can produce GO membranes with thicknesses less than 10 μm and an interlayer spacing of ~ 8 Å.[40b] GO membranes with thicknesses of 3 – 10 nm are also prepared by combining different coating techniques, e.g., contacting the support surface to the air-water interface of a GO suspension, followed by spin-coating (method I), or drop-coating followed by spin-coating of a GO solution onto the support surface (method II) (Figure 6b).[7c] It is suggested that the stacking of GO nanosheets is governed by intrinsic repulsive edge-to-edge GO sheet interactions and attractive face-to-face capillary forces created by the spin-coating. In method I, the electrostatic repulsion leads to a relatively heterogeneous GO deposition, in

which the GO stacked structure resembles islands. In method II, the GO solution-membrane contact occurs only during spin-coating, leading to highly interlocked laminates. The dense stacking occurs because the capillary interactions overcome the electrostatic forces, leading to a well – interlocked GO stacking structure.

Layer-by-layer assembly Layer-by-layer assembly of 2DMs provides an ideal way to generate a layered structure with a tuned interlayer distance by chemically modifying the 2DMs with either covalent or non-covalent interactions, controlling the thickness by varying the number of deposition cycles, and designing interlayer interactions by varying the thickness of the introduced modification species. For example, 1,3,5-benzenetricarbonyl trichloride (TMC) can covalently cross-link GO sheets by assembling sheets on top of one another in a layer-by-layer fashion on a dopamine-modified polysulfone substrate (Figure 6c).[41] The as-prepared membrane has a free interlayer spacing of approximately 1 nm and a thickness of approximately 5 – 50 GO layers. Layer-by-layer stacking in solution relies on out-of-plane (perpendicular to substrate direction) interactions to assemble materials from solution. In contrast, the air-water interface of a Langmuir-Blodgett trough offers the control of in-plane interactions of assembled materials by tuning the surface pressure.[42] At a low surface pressure, the edge to edge repulsion of GO sheets prevents them from overlapping during monolayer compression. The layers fold and wrinkle at their interacting edges at a high surface pressure, leaving the interior flat. Thus, the density of such films can be continuously tuned from dilute, close-packed to overpacked monolayers of GO sheets. Moreover, stacking of the produced layers on top of one another provides a multilayer in a well-defined layer-by-layer fashion.

Interlayer Structure Control

The separation performance of the laminates relies on their interlayer structure (such as interlayer distance, interlayer interactions, and pores), which can be controlled in different ways.

Defects are often generated as mentioned before in the preparation of 2D materials. These defects may provide permeation "gates" and shortened transport pathways through thick layered stacks (> 20 nm), achieving a higher flux.[43] On the other hand, these defects can lead to unwanted flow. When a sheet is put on top of the other, it is less likely that defects in the first layer will overlap perfectly with those in the second layer, which will result in defect annealing. In this way, escape pathways caused by the defects can be alleviated and selectivity of the membrane can be improved.[7c, 44]

The interlayer structure of laminates can be tuned by external stimuli. For example, the interlayer distance of GO membranes can be tuned by varying the relative humidity as mentioned before. Hydrophilic groups in the oxidized regions of GO can act as spacers to keep graphene planes apart. In the dry state, vacuum filtrated GO laminates (μm-thick) have a free interlayer distance of ~ 3 Å, which allows only the intercalation of a single layer of H_2O molecules. In the wetted state, the hydrophilic groups absorb large amounts of H_2O molecules, which enlarge the free interlayer distance to ~ 9 Å, providing 2D channels for the permeation of various small molecules.[38a] Moreover, upon thermal treatment of GO, irreversible defects are formed due to the decomposition of oxygen containing groups, which can be useful for certain gas separations.[7c]

Additionally, the salt concentration, pH and pressure on water permeation will all affect the interlayer channel of GO membranes.[38c] A high salt concentration can suppress the electrostatic repulsion between GO flakes in the membrane due to ionic screening effects. This leads to the shrinkage of the interlayer spacing. When the concentration of NaCl solution reaches 0.1 mol L^{-1}, water flux through the GO membrane approaches zero. At pH = 6, the water flux through the GO membrane (3 ml, 0.02 wt%) reaches a maximum. Both lower and

higher pH values decrease water flow. At low pH, protonation decreases the interlayer spacing. At high pH, the ionic strength shrinks the interlayer spacing resulting in a reduction of the flux. On the other hand, as the pressure increases, the flux increases quickly when the loading pressure is not more than 0.3 MPa; then it increases slowly and reaches a maximum at 1.0 MPa. The interlayer spacing is relatively stable at pressures ≤ 0.3 MPa. However, when the pressure is further increased, the interlayer channel cannot be sustained and begin to collapse, resulting in a smaller flux increase.

Polymers with functional groups can interact with GO to stimulate the stacking and orientation and control the interlayer distance of GO sheets of the membrane. For example, N-H, H-N-C=O, and O-C=O groups of polyether block amide (PEBA) form hydrogen bonds with oxygen-containing groups of GO, which leads to thin laminates of GO surrounded by PEBA polymeric domains. The polymeric environment enables the assembly of the thin GO laminates into membranes in random directions, where inclined and even vertical thin laminates can provide more straight and upright gas pathways than the parallel-stacked ones (Figure 7a). The randomly oriented thin laminate has a thickness of 6 – 15 nm with an interlayer spacing of ~ 3.5 Å between the GO sheets, which is in the range of the molecular kinetic diameters of industrial gases, such as CH_4 (3.8 Å), N_2 (3.6 Å), CO_2 (3.3 Å), and H_2 (2.9 Å).

For practical applications, it is desirable to develop composite membranes that consist of synthetic 2D materials (either in the form of monolayers or thin films) and a porous support membrane. The supporting membrane enhances the mechanical stability of the 2DM membranes and enables their applications in cm^2-sized separations, which otherwise is not possible. For example, to be freestanding with a cm^2 size, GO membranes need to have a thickness on the order of micrometers. Such membrane can be impermeable to gases, including helium.[40a] When the thickness decreased to less than ten nanometers and the film was supported on an anodic aluminum oxide (AAO) membrane with 20-nm pores, the

membrane showed H_2/CO_2 and H_2/N_2 mixture separation selectivities which were one to two orders of magnitude higher than those of state-of-the-art microporous membranes.[38b]

3.2. Separation Mechanism

As discussed above, gas separation with synthetic 2DMs can occur either through pores, interlayer channels, or interactions with their functional groups. Practically, the synergistic effects of two or all three factors may be responsible for the separation performance. For a better understanding, however, each separation mechanism is addressed separately in the following sections.

3.2.1. Pore Separation

Pores in materials with a size less than that of one of the separating species can allow for selective molecular sieving.[7a-c, 19, 35a, 38a, 38b, 45] For example, bilayer graphene with a pore size of ~ 3.4 Å generated by ultraviolet-induced oxidative etching showed a CO_2 (3.3 Å) / CH_4 (3.8 Å) selectivity of 6000.[7a] Materials with pores larger than the gas but smaller than its mean free path (the average distance that a gas can travel between two successive collisions with other gases) display free molecular transport behaviors (effusion). Effusive flow through a membrane is desirable for separating gas mixtures, which can be explained by the Knudsen transport of gases in nanoporous membranes as $Q = \Delta P/\sqrt{2\pi mkT}$, where Q is the gas permeance, P is the pressure, k_B is the Boltzmann constant, T is the temperature, and m is the molecular weight. Knudsen diffusion leads to the separation of gases with large differences in their molecular weights.[7b]

3.2.2. Interlayer Channel Separation

In addition to pores, interlayer channels with layered stacks can be effectively applied for gas and ion separations. To enable the interlayer channels for separation, micrometers-thick GO

membranes are normally used, which are typically impermeable to all gases because they need to go through the tortuosity of nanochannels (Figure 7b, dashed lines). On the other hand, the membrane allows unimpeded permeation of water. The graphitic regions of GO form a network of pristine-graphene capillaries, which connects with the oxidized regions within the GO laminates. Molecular dynamics simulation suggests that the involved capillary pressure is on the order of 1000 bars. The oxidized regions strongly interact with intercalating water and acts as a reservoir. The capillary-like pressure acts as a pump to drive the permeation of water through the membrane, resulting in ultrafast water permeation. In the fully hydrated state, GO membranes act as molecular sieves and block all solutes with a hydrated radius larger than 4.5 Å.[38a]

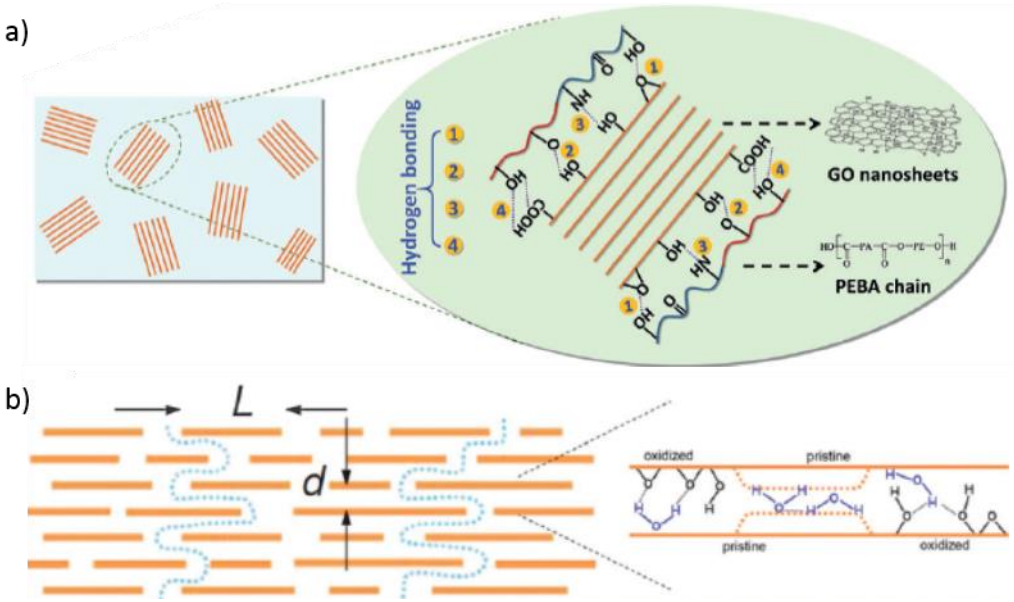

Figure 7. a) Interlayer channels of randomly-stacked GO laminates in PEBA. Reproduced with permission.[46] Copyright 2015, Wiley-VCH. Molecular transport through b) interlayer channels of GO laminates, where d is the interlayer distance. Reproduced with permission.[40a] Copyright 2012, the American Association for the Advancement of Science.

3.2.3. Functional Group-assisted Separation

In addition to pore and interlayer channel separation mechanisms, functional groups decorated on the surfaces of synthetic 2DMs are also critically important in gas and ion separations

because they can selectively interact with each other to facilitate or hinder permeation. For example, when GO with a free interlayer spacing of ~ 3.5 Å is used for separation, the permeation of CO_2 (3.3 Å) is 12 times higher than that of H_2 (2.9 Å), even though H_2 molecules are supposed to diffuse much faster than CO_2 due to its smaller kinetic diameter. This result illustrates the critical influence of the oxygen-containing groups on GO, which favorably interact with the polar individual C-O bonds on CO_2 resulting in preferential CO_2 adsorption and diffusion in the GO laminate.[46] Functional groups can also tune the permeation of ions. For example, the permeation of sodium salts with different anions is in the approximate order of NaOH > $NaHSO_4$ > $NaHCO_3$ using a GO membrane with a thickness of less than 10 μm and an interlayer spacing of ~ 8 Å.[40b] Hydroxide ions interact with carboxylate and hydroxyl groups to make them ionic and chemically active, which leads to the increase of the interlayer spacing of GO in the membranes due to electrostatic repulsion and thus facilitating the penetration of Na^+ and OH^-. In contrast, when $NaHSO_4$ solution is permeated, the H^+ ions prohibit the ionization of the oxygen-containing functional groups, which decreases the spacing of the interlayer channel and thus the permeation rate of $NaHSO_4$. When $NaHCO_3$ passes through the membrane, the chemical reactions between the HCO_3^- ions and the carboxyl groups lead to the generation of CO_2 gas, resulting in the generation of a reversed compression, which suppresses the permeation of ions.

3.3. Separation Performance

3.3.1. Gas Separation

Porous graphene layers (single or bilayer), as well as a few layers of CVD graphene and carbon nanomembranes, GO laminates, and layered stacks of 2D MOFs, have been explored for hydrogen or carbon dioxide purification, O_2/N_2 and He/N_2 separation, and water removal.

The performances of such membranes for gas separation (including water vapor) are summarized in Table 1.

DFT calculations indicate that an extremely high H_2/CH_4 selectivity of 10^{23} can be achieved for graphene membranes with 2.5 Å diameter all hydrogen-passivated pores (Entry 1, Table 1). Experiment results on a micrometer-sized bilayer graphene with randomly distributed pores of ~ 3.4 Å in size by UV-etching show a selectivity of 10^4 (Entry 2). The tens of orders of magnitude lower selectivity can be attributed to the different pore size and chemical pore termination in the simulation and the experiment.

In view of real applications, large-area membranes having preferentially ordered pores with high-densities are urgently needed for massive permeation. A valuable attempt has been realized for the separation of H_2 and CO_2 mixtures (50:50) through a bilayer graphene with millions of pores (Entry 3). Because the minimum pore size drilled can be as small as only ~ 7.6 nm, the membrane shows a Knudsen diffusion selectivity for H_2/CO_2, but the permeation rate is orders of magnitude superior to other reported values (Figure 8a).

In addition to post-drilled pores, defects and grain boundaries of CVD graphene can also be used for gas separation. A single layer of the CVD graphene supported on poly(1-methylsilyl-1-propyne) (PTMSP) shows an O_2/N_2 selectivity of 1.5 and an O_2 permeability of 730 barrer [1 barrer = 1×10^{-10} cm^3 cm/(cm^2·sec·cmHg) at standard temperature and pressure (STP)]. The selectivity can be enhanced by creating layered graphene stacks at the expense of a decreased permeability due to the increase of membrane thickness. Five layers of CVD graphene show a selectivity of 6 and O_2 permeability of 29 barrer (Entry 4). Similarly, other large-area membranes with randomly distributed pores, such as single and three layers of NBPT carbon nanomembranes, exhibit He/N_2 (H_2/N_2) selectivities of 4.10 and 11.4 (5.7 and 9.9), and He permeabilities of 7 and 1.5 m^3 m^{-2} h^{-1} bar^{-1}, respectively (Entry 5).

In contrast to the large-area of CVD graphene and CNMs, which can be directly used as separation membranes, GO and exfoliated 2D MOFs have limited lateral sizes, which are

required to be fabricated into laminates enabling massive gas permeations (Entries 6 - 10). Through structural defects, an ultrathin GO membrane (9 nm) fabricated by vacuum filtration shows H_2/CO_2 and H_2/N_2 selectivities of 3400 and 900 (Entry 6), respectively (Figure 8b). Note that the microstructures of GO can facilitate the transport of either H_2 or CO_2 (Entries 6 and 7). In addition, when several layers of stacked GO with an appropriate interlayer spacing can adopt an upright orientation in a thick film (Entry 9, Figure 7a), excellent gas permeation is observed. In contrast to GO, 2D MOFs can provide rationally designed pores, which can facilitate the transport of gas. For instance, a drop-coated poly[Zn_2(benzimidazole)$_4$ membrane on anodic aluminum oxide shows a H_2/CO_2 permeance of 2700 GPU (Entry 10), which is one order of magnitude higher than that of thin GO membranes (Entry 6, ~ 300 GPU) and conventional microporous membranes.[47]

Table 1. 2D membranes for gas separation

Entry	Membrane system[a)]	Processing method	Molecular structure[b)]	Separation [c)]	Permeance of faster species[d)]	Selectivity
1[48]	Porous graphene	Simulated all H-passivated pores	d = 2.5 Å	H_2/CH_4	1×10^{-20} mol/s Pa	10^{23}
2[7a]	Porous bilayer-graphene	UV-etching	d = 3.4 Å	H_2/CH_4	4.5×10^{-23} mol/s Pa	10000
3[7b]	Porous bilayer-graphene	Focused ion beam	d = 7.6 nm	H_2/CO_2	5×10^{-3} mol/s Pa	4.69
4[7c]	Few layer Graphene/PTMSP	CVD	1 layers 5 layers	O_2/N_2	730 Barrer 29 Barrer	1.5 6
5[44a]	NBPT-CNM/PDMS	Electron crosslinking	1 layers 3 layers	He/N_2 H_2/N_2 He/N_2 H_2/N_2	$7\ m^3\ m^{-2}\ h^{-1}\ bar^{-1}$ $2.5\ m^3\ m^{-2}h^{-1}\ bar^{-1}$ $1.5\ m^3\ m^{-2}\ h^{-1}\ bar^{-1}$ $0.94\ m^3\ m^{-2}h^{-1}\ bar^{-1}$	4.1 5.7 11.4 9.9
6[38b]	GO/AAO	Vacuum filtration	L = 9 nm	H_2/CO_2 H_2/N_2	10^{-7} mol/s Pa	3400 900
7[7c]	3 – 7 nm GO/PES	Spin-coating	L=3-7 nm	CO_2/N_2 H_2/CO_2(140°C)	100 GPU 42 GPU	20 40
8[40a]	GO membrane	spin- or spray-coated	d = 3 Å L = 1 µm	H_2O/He	1×10^{-6} Barrer	$> 10^{10}$
9[46]	GO-PEBA mixture/PVDF	Film casting	L = 5 µm	CO_2/N_2	100 Barrer	91
10[19]	poly[Zn_2(benzimidazole)$_4$ nanosheet membrane	drop-coating	d = 2.1 Å	H_2/CO_2	2700 GPU	291

[a)] PES: polyether sulfone; AAO: anodic aluminum oxide; PVDF: polyvinylidene fluoride; PTMSP: poly(1-methylsilyl-1-propyne); PDMS: polydimethylsiloxane. [b)]d: pore size or free interlayer distance; l: membrane thickness. [c)] Operated at room temperature unless otherwise noted. [d)] 1 GPU = 10^{-6} cm^3 (STP)/(cm^2 s^1 cmHg) at STP; 1 barrer = 1×10^{-10} cm^3 (STP) cm/(cm^2·sec·cmHg).

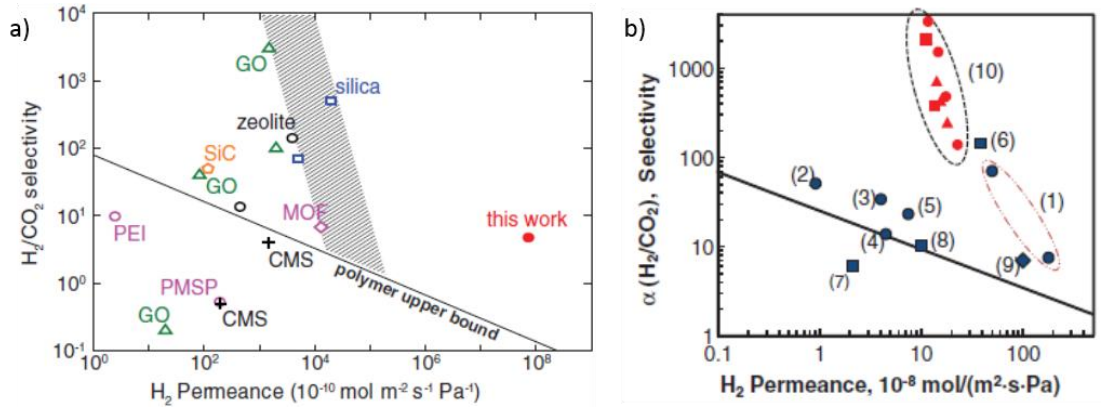

Figure 8. a) Comparison of H_2/CO_2 separation performances of porous graphene membranes (7.6-nm pore diameter with 4.0% porosity) and other membranes.[7c, 38b, 49] Reproduced with permission.[7b] Copyright 2014, American Association for the Advancement of Science. b) Comparison of ultrathin GO membranes with inorganic membranes (1-9) for H_2/CO_2 mixture (50:50) separation. The black line denotes the 2008 upper bound of the polymeric membrane for H_2/CO_2,[2] assuming the membrane thickness is 0.1 μm. Red squares, dots and triangles indicate a GO membrane with thicknesses of 1.8 nm, 9 nm, and 18 nm, respectively. Reproduced with permission.[38b] Copyright 2013, American Association for the Advancement of Science.

3.3.2. Ion Separation

The exciting finding of unimpeded water permeation through GO laminates encourages the separation of ions in aqueous solutions with synthetic 2DMs. Despite some preliminary progress, the interlayer spacing of GO membranes can be changed by external stimuli as mentioned previously. The interlayer distance change can be avoided by covalently crosslinking GO sheets with TMC (*layer-by-layer assembly*).[41] The water fluxes of the cross-linked GO membranes range between 80 and 276 L/m^2-h-MPa, which are approximately 4-10

times higher than that of most commercial nanofiltration membranes. When the cross-linked membrane is explored for salt rejection, the separation performance depended on solution concentration. The salt rejection rate decreases significantly as ionic strength (i.e., solution concentration) increases. Specifically, Na_2SO_4 rejection drops from approximately 88% at 0.1 mmol L^{-1} to nearly 26% at 10 mmol L^{-1}, whereas NaCl rejection fell from approximately 59% at 0.1 mmol L^{-1} to approximately 29% at 10 mmol L^{-1}. It can be explained by the fact that when the ion strength increases, the electrostatic repulsion between ions and the charged GO membrane decreases due to thinning of the electrostatic double layer (Debye length), thus causing the rejection rate to drop. Overall, rejection rates for salts are at reasonable levels for membranes with pores of 1 nm in size. For instance, the salt rejection is comparable to that of a CNT membrane with sub-2-nm-sized pores.[50]

3.3.3. Water Desalination

Reverse osmosis (RO) has been prevalent in industries for several decades and accounts for nearly half of the world's installed desalination capacity, mainly because it is more environmentally friendly and energy efficient than that of thermal-based desalination technologies, such as multistage flash and multiple-effect distillation. Nevertheless, current RO membranes (polyamide thin-film composite, TFC) suffer from low water permeation (~0.01–0.05 L/cm^2·day·MPa, up to 99% salt rejection), and the precise mechanism for salt rejection and water permeation are not fully understood yet due to the amorphous nature of TFC.[51] Moreover, the membranes are prone to degradation by chlorine due to extensive amide bond cleavage under chlorination-promoted hydrolysis,[52] which urgently calls for the development of new membranes.

Graphene is chemically inert and cannot be degraded by chlorine. Its atomic thinness and impermeability allow ultrafast water desalination if proper pores are introduced because the hydrated radius of ions in water is larger than the effective size of a H_2O molecule (~ 3 Å).

Based on the molecular sieving effect, the critical nanopore diameter for rejecting NaCl appears to be between 6 Å and 8 Å (hydrated radius of Na^+ is 3.6 Å), which is similar for CNTs.[53] Molecular simulation indicates that nanoporous graphene membranes (23.1 $Å^2$ hydrogenated pores and 16.3 $Å^2$ hydroxylated pores) can perform more than 99% salt rejection and provide water transport ranging from 39 to 66 $L/cm^2 \cdot day \cdot MPa$,[53b, 54] which is 2 – 3 orders of magnitude higher than in polyamide thin-film composite membranes. The chemical functional groups decorated at the periphery of the pores play an important role in determining the water desalination performance across the nanoporous graphene membrane.[53b, 55] Hydroxyl groups can roughly double the water flux due to their hydrophilic characters. The increase in water flux comes at the expense of a less consistent salt rejection performance due to the ability of the hydroxyl functional groups to substitute for water molecules in the hydration shell of the ions. In contrast, hydrophobic hydrogenated pores can reduce the water flow by imposing additional conformational order on the system, and even limited hydrogen bonding allows for higher salt rejection relative to hydroxylated pores.

Desalination across a freely suspended monocrystalline graphene with sub-nanometer-sized pores exhibits a salt rejection rate of nearly 100% and rapid water transport.[7e] In particular, water fluxes of up to 10^6 g m^{-2} s^{-1} at 40°C are measured using a pressure difference as a driving force, whereas water fluxes measured using osmotic pressure as a driving force does not exceed 70 g m^{-2} s^{-1} atm^{-1}. The high performance of this membrane opens the door for the exploration of graphene and other synthetic 2D materials for water desalination.

4. Conclusions and Outlook

The syntheses, structures, mechanical properties, and fabrication of graphene and synthetic 2DMs membranes are summarized in this report in light of their applications in gas and ion separations, as well as water desalination. Undoubtedly, the ultimate thinness and outstanding mechanical robustness of the synthetic 2DMs promise to make them essential components as

next-generation separation membranes. Despite such membranes having been studied for only several years, they have already demonstrated orders of magnitude higher permeation behavior or selectivity than those of state-of-the-art microporous membranes. For applications with a focus on permeation, synthetic 2DMs can be processed into two forms: porous membranes and layered stacks, where either pores, interlayer channels, functional groups or their combinations will dominate the separation performance.

Although significant progress has been achieved, there are still many challenges and opportunities for both the scientific community and engineers in applying 2DMs as membranes for permeation. As the starting point for the development of membranes, the materials are key and need to be synthesized and processed properly. For graphene, leak-free sheets over large areas need to be produced economically, and sub-nanometer sized pores need to be drilled with a high-density without compromising its freestanding nature. For a GO membrane, its chemical and thermal stabilities are a substantial issue, as indicated by the sensitivity to external stimuli. Covalent cross-linking of GO sheets with TMC in a layer-by-layer fashion provides a possible means to enhance the chemical stability and fix the interlayer distance of the GO membrane. However, the interlayer distance in this case is ~ 1 nm, which is larger than most standard gases and hydrated Na^+ and Cl^-, thus compromising the applications of such membrane in gas separation and water desalination. Thus, much effort should be made to realize stable GO laminates with sub-nanometer channels, e.g., desalination requires a sieve size between 3 Å and 7 Å. Moreover, in a GO laminate, the direction of permeation is perpendicular to the nanochannels, which decreases the flux rate. An achievement of vertically aligned inter-layer channels may allow for ultrafast permeation. For synthetic 2DPs, 2DSPs, and 2D MOFs, only a few examples have been synthesized thus far, and the distributions of defects within them remain to be determined. Moreover, only one material, i.e., a 2D MOF or 2DSP, was explored thus far as a sieving membrane and for gas separation solely. On the other hand, these materials have well designed pores, which will

probably be beneficial in future separation industries. Therefore, more effort to synthesize these materials and apply them as separation membranes is highly desirable. Moreover, regarding CNMs, they have random pores. Ways to create controlled nanopores with a high density without compromising the integrity and mechanical properties of the membrane are yet to be developed. Finally, leakage through defective sites within 2DMs will lead to unpredictable separation performances and therefore needs to be avoided. Layering 2DMs (with either the same or different materials) on top of one another provides a way to anneal defects and increase the separation selectivity, thus making the resulting laminates practical for gas separation and water desalination. Additionally, laminating offers a way to combine the functionalities of each layered materials and to explore their synergistic effects, which enables on-demand designs of novel functional membranes.

((References should be superscripted and appear after punctuation.[1,2] If you have used reference management software such as EndNote to prepare your manuscript, please convert the fields to plain text by selecting all text with [ctrl]+[A], then [ctrl]+[shift]+[F9]).[3–5] Please define all acronyms except IR, UV, NMR, and DNA or similar (for a complete list of acronyms not requiring definition, please see the list available on the journal homepage in our "Author Guidelines" section.))

Acknowledgements
((Acknowledgements, general annotations, funding. Other references to the title/authors can also appear here, such as "Author 1 and Author 2 contributed equally to this work."))

Received: ((will be filled in by the editorial staff))
Revised: ((will be filled in by the editorial staff))
Published online: ((will be filled in by the editorial staff))

[1] D. L. Gin, R. D. Noble, *Science* **2011**, *332*, 674.
[2] L. M. Robeson, *J. Membrane Sci.* **2008**, *320*, 390.

[3] J. Gascon, F. Kapteijn, B. Zornoza, V. Sebastián, C. Casado, J. Coronas, *Chem. Mat.* **2012**, *24*, 2829.

[4] a) B. J. Hinds, N. Chopra, T. Rantell, R. Andrews, V. Gavalas, L. G. Bachas, *Science* **2004**, *303*, 62; b) J.-P. Salvetat, G. A. D. Briggs, J.-M. Bonard, R. R. Bacsa, A. J. Kulik, T. Stöckli, N. A. Burnham, L. Forró, *Phys. Rev. Lett.* **1999**, *82*, 944.

[5] a) K. S. Novoselov, A. K. Geim, S. V. Morozov, D. Jiang, Y. Zhang, S. V. Dubonos, I. V. Grigorieva, A. A. Firsov, *Science* **2004**, *306*, 666; b) Y. Zhu, S. Murali, W. Cai, X. Li, J. W. Suk, J. R. Potts, R. S. Ruoff, *Adv. Mater.* **2010**, *22*, 3906; c) J. Sakamoto, J. van Heijst, O. Lukin, A. D. Schlüter, *Angew. Chem. Int. Edit.* **2009**, *48*, 1030; d) A. Turchanin, A. Golzhauser, *Prog. Surf. Sci.* **2012**, *87*, 108; e) P. Payamyar, B. T. King, H. C. Ottinger, A. D. Schluter, *Chem. Commun.* **2015**; f) X. Zhuang, F. Zhang, D. Wu, X. Feng, *Adv. Mater.* **2014**, *26*, 3081.

[6] C. Lee, X. Wei, J. W. Kysar, J. Hone, *Science* **2008**, *321*, 385.

[7] a) S. P. Koenig, L. D. Wang, J. Pellegrino, J. S. Bunch, *Nature Nanotechnol.* **2012**, *7*, 728; b) K. Celebi, J. Buchheim, R. M. Wyss, A. Droudian, P. Gasser, I. Shorubalko, J. I. Kye, C. Lee, H. G. Park, *Science* **2014**, *344*, 289; c) H. W. Kim, H. W. Yoon, S. M. Yoon, B. M. Yoo, B. K. Ahn, Y. H. Cho, H. J. Shin, H. Yang, U. Paik, S. Kwon, J. Y. Choi, H. B. Park, *Science* **2013**, *342*, 91; d) S. C. O'Hern, C. A. Stewart, M. S. H. Boutilier, J. C. Idrobo, S. Bhaviripudi, S. K. Das, J. Kong, T. Laoui, M. Atieh, R. Karnik, *Acs Nano* **2012**, *6*, 10130; e) S. P. Surwade, S. N. Smirnov, I. V. Vlassiouk, R. R. Unocic, G. M. Veith, S. Dai, S. M. Mahurin, *Nature Nanotechnol.* **2015**, *10*, 459.

[8] a) Y. Hao, M. S. Bharathi, L. Wang, Y. Liu, H. Chen, S. Nie, X. Wang, H. Chou, C. Tan, B. Fallahazad, H. Ramanarayan, C. W. Magnuson, E. Tutuc, B. I. Yakobson, K. F. McCarty, Y.-W. Zhang, P. Kim, J. Hone, L. Colombo, R. S. Ruoff, *Science* **2013**, *342*, 720; b) J.-H. Lee, E. K. Lee, W.-J. Joo, Y. Jang, B.-S. Kim, J. Y. Lim, S.-H. Choi, S. J. Ahn, J. R. Ahn, M.-H. Park, C.-W. Yang, B. L. Choi, S.-W. Hwang, D. Whang, *Science* **2014**, *344*, 286.

[9] S. Bae, H. Kim, Y. Lee, X. Xu, J.-S. Park, Y. Zheng, J. Balakrishnan, T. Lei, H. Ri Kim, Y. I. Song, Y.-J. Kim, K. S. Kim, B. Ozyilmaz, J.-H. Ahn, B. H. Hong, S. Iijima, *Nat Nano* **2010**, *5*, 574.

[10] a) X. Li, Y. Zhu, W. Cai, M. Borysiak, B. Han, D. Chen, R. D. Piner, L. Colombo, R. S. Ruoff, *Nano Lett.* **2009**, *9*, 4359; b) K. S. Kim, Y. Zhao, H. Jang, S. Y. Lee, J. M. Kim, K. S. Kim, J.-H. Ahn, P. Kim, J.-Y. Choi, B. H. Hong, *Nature* **2009**, *457*, 706.

[11] V. Berry, *Carbon* **2013**, *62*, 1.

[12] K. Erickson, R. Erni, Z. Lee, N. Alem, W. Gannett, A. Zettl, *Adv. Mater.* **2010**, *22*, 4467.

[13] J. W. Suk, R. D. Piner, J. An, R. S. Ruoff, *ACS Nano* **2010**, *4*, 6557.

[14] a) D. R. Dreyer, S. Park, C. W. Bielawski, R. S. Ruoff, *Chem. Soc. Rev.* **2010**, *39*, 228; b) S. Eigler, A. Hirsch, *Angew. Chem. Int. Edit.* **2014**, *53*, 7720; c) F. Perrozzi, S. Prezioso, L. Ottaviano, *J. Phys.-Condens. Mat.* **2015**, *27*.

[15] W. S. Hummers, R. E. Offeman, *J. Am. Chem. Soc.* **1958**, *80*, 1339.

[16] P. Kissel, R. Erni, W. B. Schweizer, M. D. Rossell, B. T. King, T. Bauer, S. Götzinger, A. D. Schlüter, J. Sakamoto, *Nat Chem* **2012**, *4*, 287.

[17] P. Kissel, D. J. Murray, W. J. Wulftange, V. J. Catalano, B. T. King, *Nat Chem* **2014**, *6*, 774.

[18] a) D. J. Murray, D. D. Patterson, P. Payamyar, R. Bhola, W. Song, M. Lackinger, A. D. Schlüter, B. T. King, *J. Am. Chem. Soc.* **2015**, *137*, 3450; b) Z. Zheng, L. Opilik, F. Schiffmann, W. Liu, G. Bergamini, P. Ceroni, L.-T. Lee, A. Schütz, J. Sakamoto, R. Zenobi, J. VandeVondele, A. D. Schlüter, *J. Am. Chem. Soc.* **2014**, *136*, 6103.

[19] Y. Peng, Y. S. Li, Y. J. Ban, H. Jin, W. M. Jiao, X. L. Liu, W. S. Yang, *Science* **2014**, *346*, 1356.

[20] Z. Zheng, C. S. Ruiz-Vargas, T. Bauer, A. Rossi, P. Payamyar, A. Schütz, A. Stemmer, J. Sakamoto, A. D. Schlüter, *Macromol. Rapid Comm.* **2013**, *34*, 1670.

[21] R. Dong, M. Pfeffermann, H. Liang, Z. Zheng, X. Zhu, J. Zhang, X. Feng, *Angew. Chem. Int. Edit.* **2015**, *54*, 12058.

[22] a) M. Bieri, M. Treier, J. Cai, K. Ait-Mansour, P. Ruffieux, O. Groning, P. Groning, M. Kastler, R. Rieger, X. Feng, K. Mullen, R. Fasel, *Chem. Commun.* **2009**, 6919; b) J. Liu, P. Ruffieux, X. Feng, K. Mullen, R. Fasel, *Chem. Commun.* **2014**, *50*, 11200; c) L. Grill, M. Dyer, L. Lafferentz, M. Persson, M. V. Peters, S. Hecht, *Nat Nano* **2007**, *2*, 687.

[23] a) P. Payamyar, K. Kaja, C. Ruiz-Vargas, A. Stemmer, D. J. Murray, C. J. Johnson, B. T. King, F. Schiffmann, J. VandeVondele, A. Renn, S. Götzinger, P. Ceroni, A. Schütz, L.-T. Lee, Z. Zheng, J. Sakamoto, A. D. Schlüter, *Adv. Mater.* **2014**, *26*, 2052; b) Y. Chen, M. Li, P. Payamyar, Z. Zheng, J. Sakamoto, A. D. Schlüter, *ACS Macro Letters* **2014**, *3*, 153; c) P. Payamyar, M. Servalli, T. Hungerland, A. P. Schütz, Z. Zheng, A. Borgschulte, A. D. Schlüter, *Macromol. Rapid Comm.* **2015**, *36*, 151.

[24] a) T. Bauer, Z. Zheng, A. Renn, R. Enning, A. Stemmer, J. Sakamoto, A. D. Schlüter, *Angew. Chem. Int. Edit.* **2011**, *50*, 7879; b) R. Sakamoto, K. Hoshiko, Q. Liu, T. Yagi, T. Nagayama, S. Kusaka, M. Tsuchiya, Y. Kitagawa, W.-Y. Wong, H. Nishihara, *Nat Commun* **2015**, *6*, 6713; c) T. Kambe, R. Sakamoto, K. Hoshiko, K. Takada, M. Miyachi, J.-H. Ryu, S. Sasaki, J. Kim, K. Nakazato, M. Takata, H. Nishihara, *J. Am. Chem. Soc.* **2013**, *135*, 2462; d) R. Makiura, S. Motoyama, Y. Umemura, H. Yamanaka, O. Sakata, H. Kitagawa, *Nat Mater* **2010**, *9*, 565; e) S. Motoyama, R. Makiura, O. Sakata, H. Kitagawa, *J. Am. Chem. Soc.* **2011**, *133*, 5640; f) R. Makiura, O. Konovalov, *Scientific Reports* **2013**, *3*, 2506; g) P. Amo-Ochoa, L. Welte, R. Gonzalez-Prieto, P. J. Sanz Miguel, C. J. Gomez-Garcia, E. Mateo-Marti, S. Delgado, J. Gomez-Herrero, F. Zamora, *Chem. Commun.* **2010**, *46*, 3262; h) C. Hermosa, B. R. Horrocks, J. I. Martinez, F. Liscio, J. Gomez-Herrero, F. Zamora, *Chem. Sci.* **2015**, *6*, 2553; i) A. Gallego, C. Hermosa, O. Castillo, I. Berlanga, C. J. Gómez-García, E. Mateo-Martí, J. I. Martínez, F. Flores, C. Gómez-Navarro, J. Gómez-Herrero, S. Delgado, F. Zamora, *Adv. Mater.* **2013**, *25*, 2141; j) M. Pfeffermann, R. Dong, R. Graf, W. Zajaczkowski, T. Gorelik, W. Pisula, A. Narita, K. Müllen, X. Feng, *J. Am. Chem. Soc.* **2015**.

[25] R. Sakamoto, T. Kambe, S. Tsukada, K. Takada, K. Hoshiko, Y. Kitagawa, M. Okumura, H. Nishihara, *Inorg. Chem.* **2013**, *52*, 7411.

[26] a) E. S. Andreiadis, P.-A. Jacques, P. D. Tran, A. Leyris, M. Chavarot-Kerlidou, B. Jousselme, M. Matheron, J. Pécaut, S. Palacin, M. Fontecave, V. Artero, *Nat Chem* **2013**, *5*, 48; b) Y. Ito, W. Cong, T. Fujita, Z. Tang, M. Chen, *Angew. Chem. Int. Edit.* **2015**, *54*, 2131.

[27] a) P. Angelova, H. Vieker, N.-E. Weber, D. Matei, O. Reimer, I. Meier, S. Kurasch, J. Biskupek, D. Lorbach, K. Wunderlich, L. Chen, A. Terfort, M. Klapper, K. Müllen, U. Kaiser, A. Gölzhäuser, A. Turchanin, *ACS Nano* **2013**, *7*, 6489; b) W. Eck, A. Küller, M. Grunze, B. Völkel, A. Gölzhäuser, *Adv. Mater.* **2005**, *17*, 2583; c) X. H. Zhang, C. Neumann, P. Angelova, A. Beyer, A. Golzhauser, *Langmuir* **2014**, *30*, 8221; d) A. Turchanin, A. Beyer, C. T. Nottbohm, X. Zhang, R. Stosch, A. Sologubenko, J. Mayer, P. Hinze, T. Weimann, A. Gölzhäuser, *Adv. Mater.* **2009**, *21*, 1233.

[28] Z. Zheng, C. T. Nottbohm, A. Turchanin, H. Muzik, A. Beyer, M. Heilemann, M. Sauer, A. Gölzhäuser, *Angew. Chem. Int. Edit.* **2010**, *49*, 8493.

[29] Z. Zheng, X. Zhang, C. Neumann, D. Emmrich, A. Winter, H. Vieker, W. Liu, M. Lensen, A. Golzhauser, A. Turchanin, *Nanoscale* **2015**, *7*, 13393.

[30] a) M. J. Schultz, X. Zhang, S. Unarunotai, D.-Y. Khang, Q. Cao, C. Wang, C. Lei, S. MacLaren, J. A. N. T. Soares, I. Petrov, J. S. Moore, J. A. Rogers, *P. Natl. Acad. Sci.*

2008, *105*, 7353; b) S. Schrettl, C. Stefaniu, C. Schwieger, G. Pasche, E. Oveisi, Y. Fontana, A. F. I. Morral, J. Reguera, R. Petraglia, C. Corminboeuf, G. Brezesinski, H. Frauenrath, *Nat. Chem.* **2014**, *6*, 468; c) I. Levesque, J. R. Neabo, S. Rondeau-Gagne, C. Vigier-Carriere, M. Daigle, J.-F. Morin, *Chem. Sci.* **2014**, *5*, 831.

[31] a) M. D. Fischbein, M. Drndić, *Appl. Phys. Lett.* **2008**, *93*, 113107; b) S. Garaj, W. Hubbard, A. Reina, J. Kong, D. Branton, J. A. Golovchenko, *Nature* **2010**, *467*, 190.

[32] G. Diankov, M. Neumann, D. Goldhaber-Gordon, *ACS Nano* **2013**, *7*, 1324.

[33] a) J. Bai, X. Zhong, S. Jiang, Y. Huang, X. Duan, *Nat Nano* **2010**, *5*, 190; b) N. S. Safron, A. S. Brewer, M. S. Arnold, *Small* **2011**, *7*, 492.

[34] J. Liu, H. Cai, X. Yu, K. Zhang, X. Li, J. Li, N. Pan, Q. Shi, Y. Luo, X. Wang, *J. Phys. Chem. C* **2012**, *116*, 15741.

[35] a) S. C. O'Hern, M. S. H. Boutilier, J. C. Idrobo, Y. Song, J. Kong, T. Laoui, M. Atieh, R. Karnik, *Nano Lett.* **2014**, *14*, 1234; b) C. J. Russo, J. A. Golovchenko, *P. Natl. Acad. Sci.* **2012**, *109*, 5953.

[36] D. Fox, A. O'Neill, D. Zhou, M. Boese, J. N. Coleman, H. Z. Zhang, *Appl. Phys. Lett.* **2011**, *98*, 243117.

[37] G. Liu, W. Jin, N. Xu, *Chem. Soc. Rev.* **2015**, *44*, 5016.

[38] a) R. K. Joshi, P. Carbone, F. C. Wang, V. G. Kravets, Y. Su, I. V. Grigorieva, H. A. Wu, A. K. Geim, R. R. Nair, *Science* **2014**, *343*, 752; b) H. Li, Z. N. Song, X. J. Zhang, Y. Huang, S. G. Li, Y. T. Mao, H. J. Ploehn, Y. Bao, M. Yu, *Science* **2013**, *342*, 95; c) H. B. Huang, Y. Y. Mao, Y. L. Ying, Y. Liu, L. W. Sun, X. S. Peng, *Chem. Commun.* **2013**, *49*, 5963; d) C.-H. Tsou, Q.-F. An, S.-C. Lo, M. De Guzman, W.-S. Hung, C.-C. Hu, K.-R. Lee, J.-Y. Lai, *J. Membrane Sci.* **2015**, *477*, 93.

[39] K. Raidongia, J. Huang, *J. Am. Chem. Soc.* **2012**, *134*, 16528.

[40] a) R. R. Nair, H. A. Wu, P. N. Jayaram, I. V. Grigorieva, A. K. Geim, *Science* **2012**, *335*, 442; b) P. Z. Sun, M. Zhu, K. L. Wang, M. L. Zhong, J. Q. Wei, D. H. Wu, Z. P. Xu, H. W. Zhu, *ACS Nano* **2013**, *7*, 428.

[41] M. Hu, B. Mi, *Environ. Sci. Technol.* **2013**, *47*, 3715.

[42] L. J. Cote, F. Kim, J. Huang, *J. Am. Chem. Soc.* **2009**, *131*, 1043.

[43] Y. Han, Z. Xu, C. Gao, *Adv. Funct. Mater.* **2013**, *23*, 3693.

[44] a) M. Ai, S. Shishatskiy, J. Wind, X. H. Zhang, C. T. Nottbohm, N. Mellech, A. Winter, H. Vieker, J. Qiu, K. J. Dietz, A. Golzhauser, A. Beyer, *Adv. Mater.* **2014**, *26*, 3421; b) M. S. H. Boutilier, C. Z. Sun, S. C. O'Hern, H. Au, N. G. Hadjiconstantinou, R. Karnik, *Acs Nano* **2014**, *8*, 841.

[45] Z. P. Smith, B. D. Freeman, *Angew. Chem. Int. Edit.* **2014**, *53*, 10286.

[46] J. Shen, G. P. Liu, K. Huang, W. Q. Jin, K. R. Lee, N. P. Xu, *Angew. Chem. Int. Edit.* **2015**, *54*, 578.

[47] Y. S. Lin, I. Kumakiri, B. N. Nair, H. Alsyouri, *Separation & Purification Reviews* **2002**, *31*, 229.

[48] D. E. Jiang, V. R. Cooper, S. Dai, *Nano Lett.* **2009**, *9*, 4019.

[49] K. Nagai, A. Higuchi, T. Nakagawa, *Journal of Polymer Science Part B-Polymer Physics* **1995**, *33*, 289.

[50] F. Fornasiero, H. G. Park, J. K. Holt, M. Stadermann, C. P. Grigoropoulos, A. Noy, O. Bakajin, *P. Natl. Acad. Sci.* **2008**, *105*, 17250.

[51] a) L. Malaeb, G. M. Ayoub, *Desalination* **2011**, *267*, 1; b) E. Harder, D. E. Walters, Y. D. Bodnar, R. S. Faibish, B. Roux, *The Journal of Physical Chemistry B* **2009**, *113*, 10177; c) D. Cohen-Tanugi, J. C. Grossman, *Desalination* **2015**, *366*, 59; d) P. S. Goh, A. F. Ismail, *Desalination* **2015**, *356*, 115.

[52] V. T. Do, C. Y. Tang, M. Reinhard, J. O. Leckie, *Environ. Sci. Technol.* **2012**, *46*, 13184.

[53] a) B. Corry, *J. Phys. Chem. B* **2008**, *112*, 1427; b) D. Cohen-Tanugi, J. C. Grossman, *Nano Lett.* **2012**, *12*, 3602.
[54] D. Cohen-Tanugi, S. H. Dave, R. K. McGovern, J. H. Lienhard, J. C. Grossman, in *Technologies for Sustainability (SusTech), 2013 1st IEEE Conference on*, **2013**, pp. 272.
[55] a) K. Sint, B. Wang, P. Král, *J. Am. Chem. Soc.* **2008**, *130*, 16448; b) D. Konatham, J. Yu, T. A. Ho, A. Striolo, *Langmuir* **2013**, *29*, 11884.

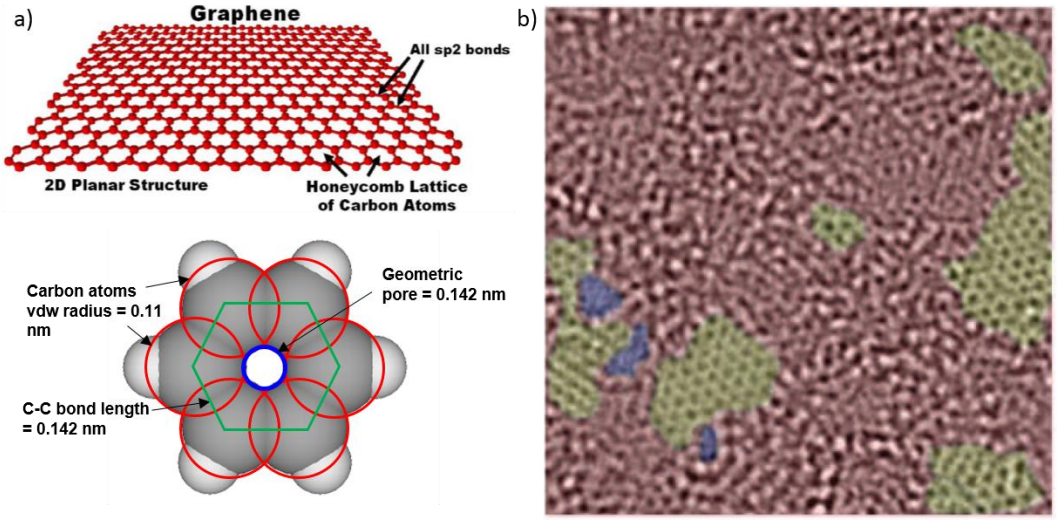

Figure 1. a) Graphene lattice structure. Reproduced with permission.[11] Copyright 2013, Elsevier. b) TEM image of suspended GO sheet; holes, graphite areas, and oxidized regions are marked in blue, yellow, and red, respectively. Reproduced with permission.[12] Copyright 2010, Wiley-VCH.

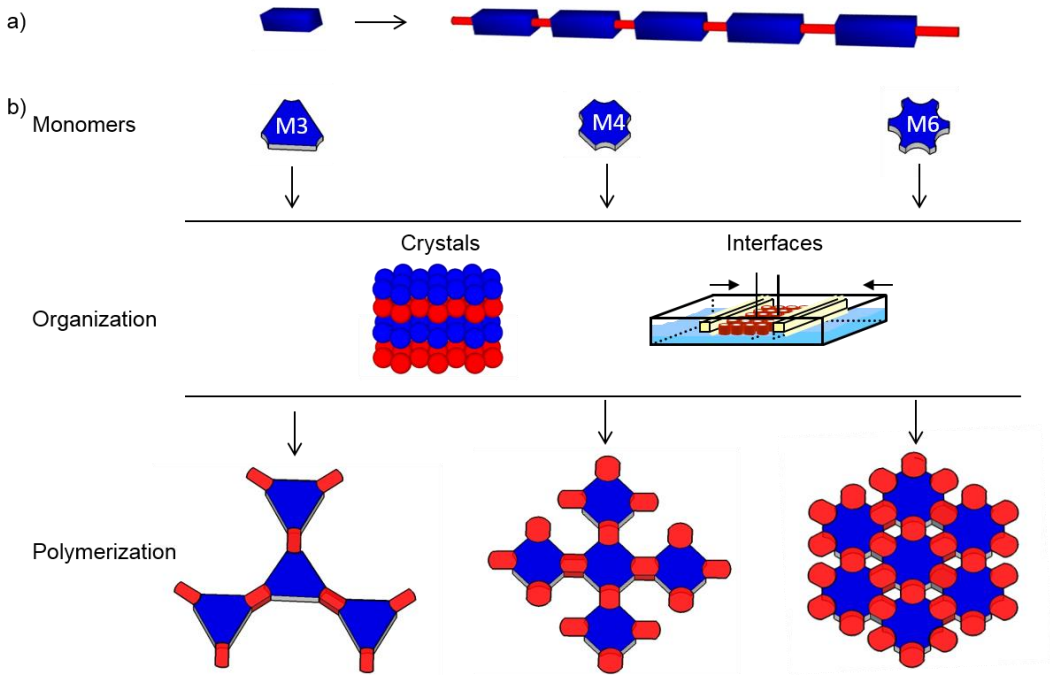

Figure 2. Schematic illustration for the synthesis of a) linear polymers and b) 2DPs/2DSPs with rigid and symmetric monomers at the interfaces. Crystal and air-water interfaces are used as examples to confine monomers in two dimensions.

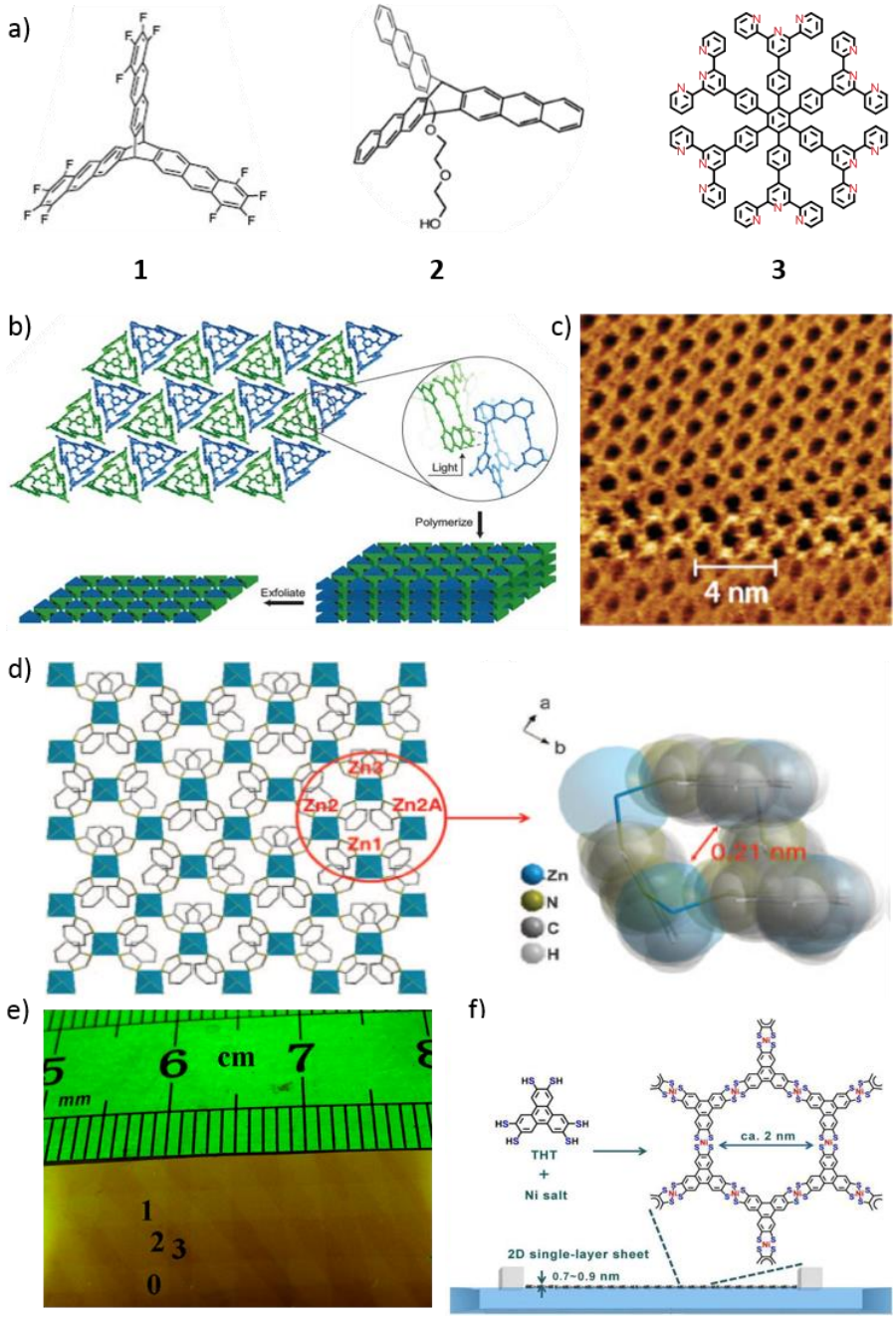

Figure 3. Representative examples of 2DPs, 2DSPs, and 2DMOFs. a) Chemical structure of monomers **1** – **3**.[17-18] b) Schematic illustration to achieve 2DPs with top-down exfoliation from laminar crystals. Reproduced with permission.[16] Copyright 2012, Macmillan Publishers Limited. c) Scanning tunneling microscope image of a 2DP from monomer **2** on highly oriented pyrolytic graphite (HOPG). Reproduced with permission.[18a] Copyright 2014, American Chemical Society. d) Structure and pore size illustrations of a 2D Zn_2(benzimidazole)$_4$. Reproduced with permission.[19] Copyright 2015, the American Association for the Advancement of Science. e) Optical microscopy image of stacked 2DSP stripes from monomer **3**. The number of 2DSP strips is indicated. Reproduced with permission.[20] Copyright 2013, Wiley-VCH. f) Synthesis of a 2DSP composed of triphenylene-fused nickel bis(dithiolene) complexes through the Langmuir-Blodgett method at an air/water interface. Reproduced with permission.[21] Copyright 2015, Wiley-VCH.

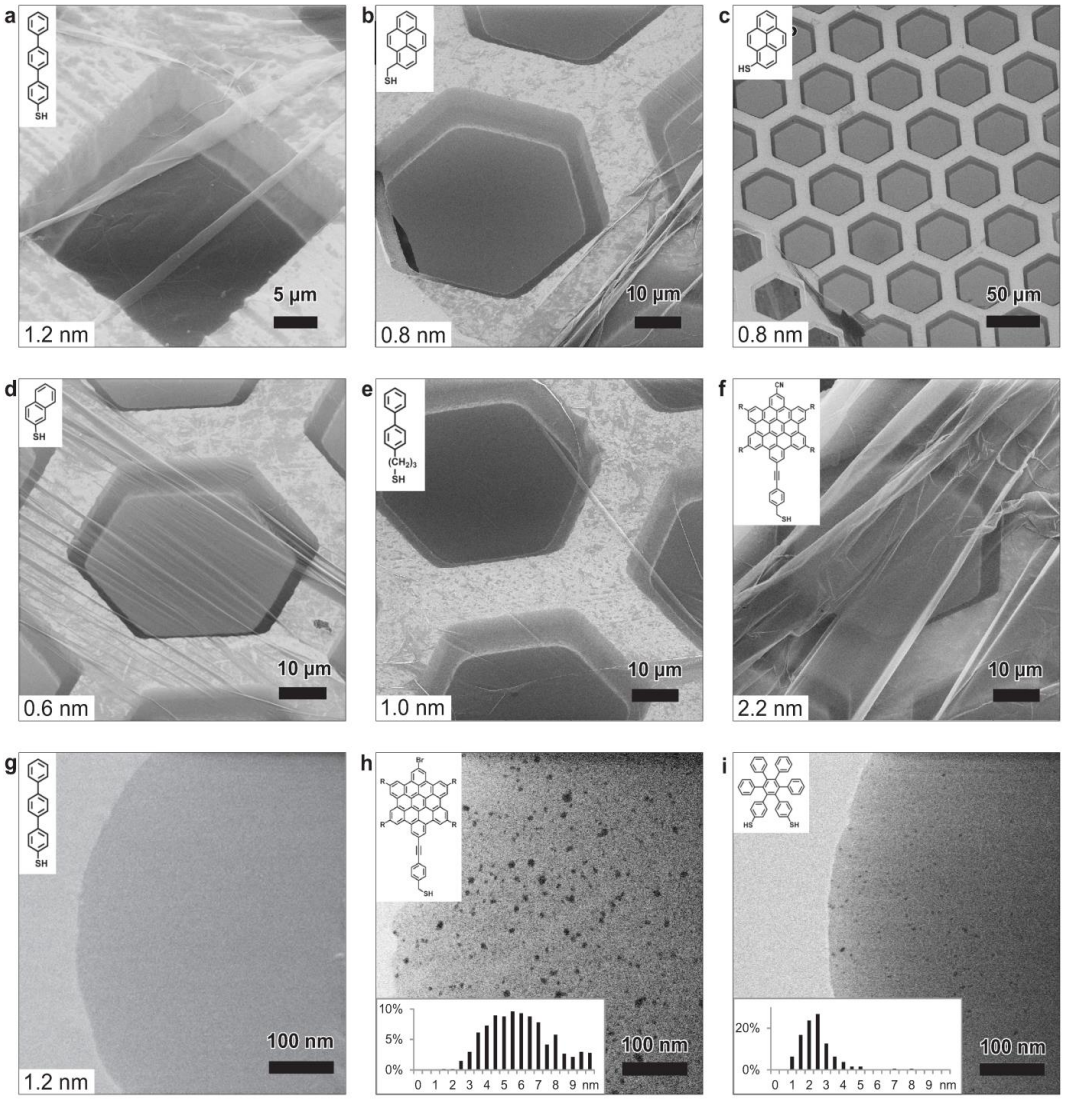

Figure 4. Helium ion microscope (HIM) micrographs of free-standing CNMs. The upper left insets show the precursor molecules. The CNM in (a) is suspended over a gold TEM grid. CNMs in (b-f) are over copper grids and CNMs in (g-i) are over Cu grids with thin carbon films. The numbers in the lower left corners indicate the CNM thicknesses. HIM images (h and i) show CNMs with nanopores; the lower insets show the respective distributions (in %) of the pore diameters (in nm). Reproduced with permission.[27a] Copyright 2013, American Chemical Society.

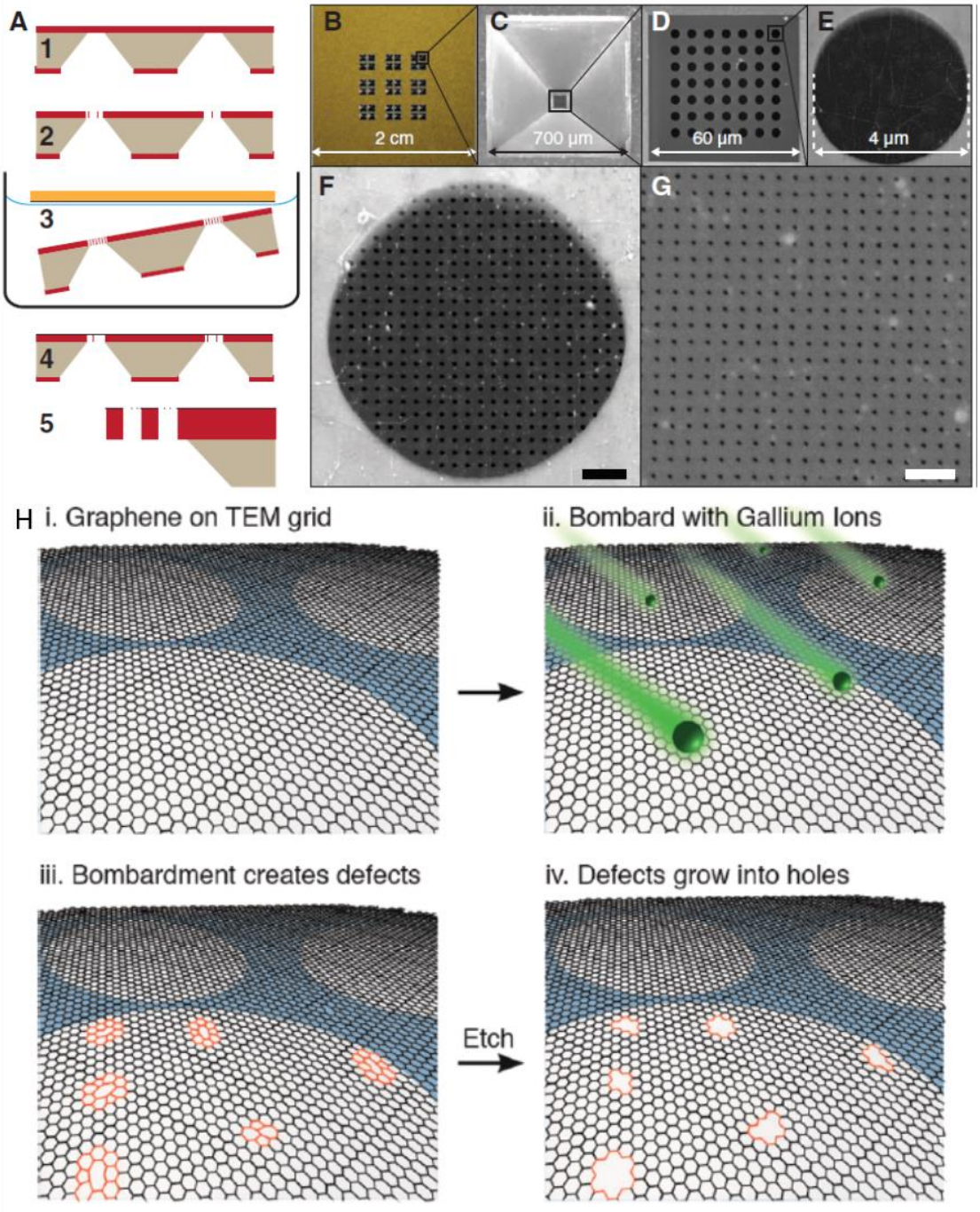

Figure 5. Process to create ordered (A-G) and randomly-distributed (H) pores in graphene membranes. (A) Schematic of the porous graphene fabrication process. Step 1: Freestanding SiNx membrane formation. Step 2: Microscale pore formation through the SiNx membrane. Step 3: Graphene transfer. Step 4: Graphene surface cleanup. Step 5: physical perforation of graphene (by means of Ga- and He-based FIB drilling). (B) Photograph (bottom view) of a full-membrane structure. (C) Bottom view SEM image of the SiNx membrane. (D to G) Top view SEM images of (D) porous freestanding SiNx window before graphene transfer, (E) freestanding graphene on SiNx open pores, (F) 50-nm-wide apertures on the freestanding graphene (scale bar, 500 nm), and (G) 7.6-nm-wide apertures (scale bar = 100 nm). Reproduced with permission.[7b] Copyright 2014, American Association for the Advancement of Science. H) Subnanometer pores in graphene are created by ion bombardment followed by chemical oxidation. Reproduced with permission.[35a] Copyright 2014, American Chemical Society.

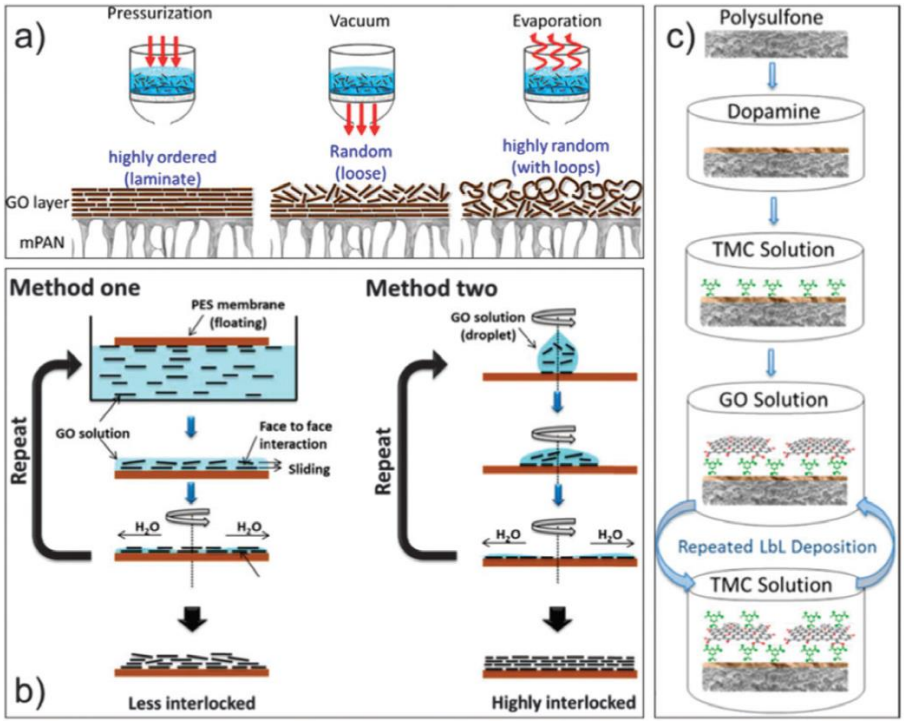

Figure 6. Processing methods for the fabrication of stacked layers by different methods: (a) pressure-assisted self-assembly, vacuum-assisted self-assembly, and evaporation-assisted self-assembly, (b) spin-coating methods, and (c) layer-by-layer method. Reproduced with permission.[37] Copyright 2015, Royal Society of Chemistry.

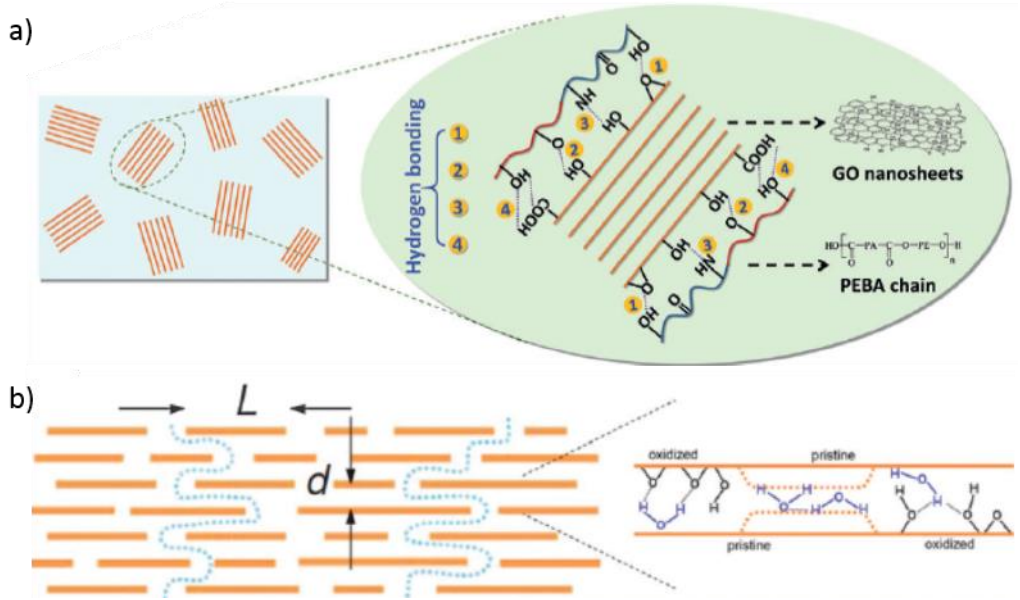

Figure 7. a) Interlayer channels of randomly-stacked GO laminates in PEBA. Reproduced with permission.[46] Copyright 2015, Wiley-VCH. Molecular transport through b) interlayer channels of GO laminates, where d is the interlayer distance. Reproduced with permission.[40a] Copyright 2012, the American Association for the Advancement of Science.

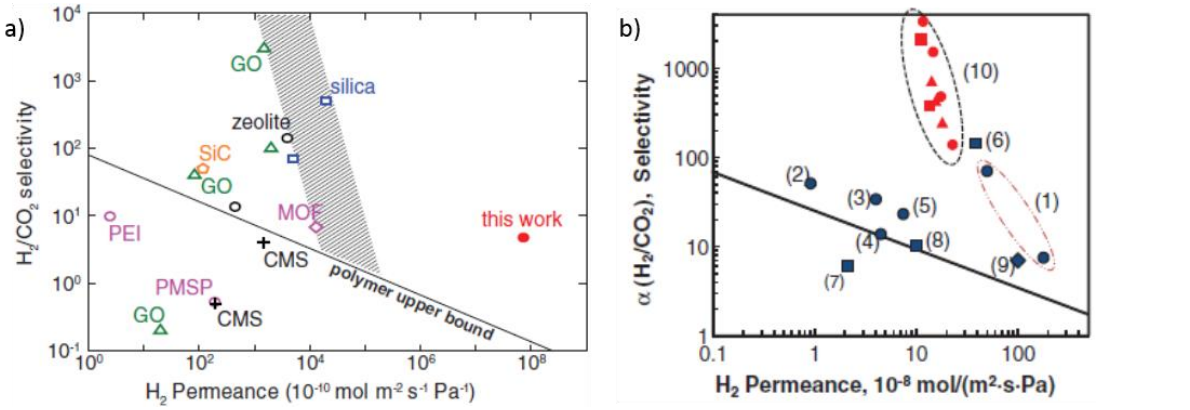

Figure 8. a) Comparison of H_2/CO_2 separation performances of porous graphene membranes (7.6-nm pore diameter with 4.0% porosity) and other membranes.[7c, 38b, 49] Reproduced with permission.[7b] Copyright 2014, American Association for the Advancement of Science. b) Comparison of ultrathin GO membranes with inorganic membranes (1-9) for H_2/CO_2 mixture (50:50) separation. The black line denotes the 2008 upper bound of the polymeric membrane for H_2/CO_2,[2] assuming the membrane thickness is 0.1 μm. Red squares, dots and triangles indicate a GO membrane with thicknesses of 1.8 nm, 9 nm, and 18 nm, respectively. Reproduced with permission.[38b] Copyright 2013, American Association for the Advancement of Science.

Table 1. 2D membranes for gas separation

Entry	Membrane system[a)]	Processing method	Molecular structure[b)]	Separation [c)]	Permeance of faster species[d)]	Selectivity
1[48]	Porous graphene	Simulated all H-passivated pores	d = 2.5 Å	H_2/CH_4	1×10^{-20} mol/s Pa	10^{23}
2[7a]	Porous bilayer-graphene	UV-etching	d = 3.4 Å	H_2/CH_4	4.5×10^{-23} mol/s Pa	10000
3[7b]	Porous bilayer-graphene	Focused ion beam	d = 7.6 nm	H_2/CO_2	5×10^{-3} mol/s Pa	4.69
4[7c]	Few layer Graphene/PTMSP	CVD	1 layers 5 layers	O_2/N_2	730 Barrer 29 Barrer	1.5 6
5[44a]	NBPT-CNM/PDMS	Electron crosslinking	1 layers 3 layers	He/N_2 H_2/N_2 He/N_2 H_2/N_2	7 $m^3 m^{-2} h^{-1} bar^{-1}$ 2.5 $m^3 m^{-2} h^{-1} bar^{-1}$ 1.5 $m^3 m^{-2} h^{-1} bar^{-1}$ 0.94 $m^3 m^{-2} h^{-1} bar^{-1}$	4.1 5.7 11.4 9.9
6[38b]	GO/AAO	Vacuum filtration	L = 9 nm	H_2/CO_2 H_2/N_2	10^{-7} mol/s Pa	3400 900
7[7c]	3 – 7 nm GO/PES	Spin-coating	L=3-7 nm	CO_2/N_2 H_2/CO_2(140°C)	100 GPU 42 GPU	20 40
8[40a]	GO membrane	spin- or spray-coated	d = 3 Å L = 1 μm	H_2O/He	1×10^{-6} Barrer	$> 10^{10}$
9[46]	GO-PEBA mixture/PVDF	Film casting	L = 5 μm	CO_2/N_2	100 Barrer	91
10[19]	poly[Zn_2(benzimidazole)$_4$ nanosheet membrane	drop-coating	d = 2.1 Å	H_2/CO_2	2700 GPU	291

[a)]PES: polyether sulfone; AAO: anodic aluminum oxide; PVDF: polyvinylidene fluoride; PTMSP: poly(1-methylsilyl-1-propyne); PDMS: polydimethylsiloxane. [b)]d: pore size or free interlayer distance; l: membrane thickness. [c)] Operated at room temperature unless otherwise

noted. [d] 1 GPU = 10^{-6} cm^3 (STP)/(cm^2 s^1 cmHg) at STP; 1 barrer = 1×10^{-10} cm^3 (STP) cm/(cm^2·sec·cmHg).